International Journal of Mechanical Sciences 212 (2021) 106844

Contents lists available at ScienceDirect

International Journal of Mechanical Sciences

journal homepage: www.elsevier.com/locate/ijmecsci

Progressive wear based tool failure analysis during dry and MQL assisted sustainable micro-milling

Suman Saha, Sankha Deb, Partha Pratim Bandyopadhyay *

Department of Mechanical Engineering, Indian Institute of Technology Kharagpur, Kharagpur, West Bengal, India, 721302

ARTICLE INFO

Keywords:
Micro-milling
Edge radius
Tool wear
Minimum Uncut Chip Thickness
Minimum Quantity Lubrication
Cutting forces

ABSTRACT

Micro-milling tools suffer high wear rate and early edge-chipping owing to their small sizes. Mechanism of various wear modes of a coated tool with the progression of micro-milling along with the conditions for their onset was not systematically explored in literature. To understand the edge-chipping scenario with the progression of wear, a comprehensive tribological analysis is presented in this article considering the cumulative effects of process mechanics, material deformation mechanism, tool geometry, lubrication, and process parameters during micro-milling of Ti-6Al-4V using 500 μm TiAlN-coated WC/6Co end-mills. The apparent friction coefficient at the chip-tool-workpiece interface remains very high, in the range of 0.97 – 0.84 in dry micro-milling that reduces to 0.60 – 0.50 under sustainable minimum quantity lubrication (MQL). When a fresh tool is engaged, it undergoes rapid wear for initial 15 mm length of cut. Thereafter, the tool undergoes gradual non-adhesive wear for another 40 – 70 mm cut. As the edge radius increases with machining time, the corresponding minimum uncut chip thickness (h_{min}) also increases proportionally. When h_{min} exceeds 12% (for MQL) or 34% (for dry) of the set feed per flute, strong adhesion occurs at the cutting edge, and the process is dominated by the non-cutting passes. Normal stresses within the ploughing-dominant region also remain reasonably high (10 – 18 GPa). Initially the coating, and thereafter the adhered layer, helps sustaining such high normal stresses. Once the adhered layer dislodges, the exposed substrate fails to sustain high stresses leading to edge-chipping. As compared to dry micro-milling, application of MQL helps decreasing abrasion rate, assisting in chip-evacuation, discouraging adhesion, and extending the tool-life; however, the same unfavourably increases the intensity of stresses within the ploughing-dominant region making the tool-tip more vulnerable to chipping.

1. Introduction

Presence of physical contact and relative velocities under high pressure between chip-tool-workpiece lead to the gradual loss of material from the cutting edges during machining. The cutting edges can also fail catastrophically whenever the normal stress acting on the tool exceeds the tolerable strength of the corresponding tool material [1]. Reduction of the tool wear rate and prevention of tool failure are challenges for every tool-based cutting process. As a subtractive micro-fabrication process, mechanical micro-milling process also employs a solid cutter having one or more cutting edges in order to gradually remove material from the workpiece in the form of micro-chips. Commercial micro-milling tools typically have diameter in 100 – 1000 μm range. Substrate material of such tools vary from single- or poly-crystalline diamond, cermet, cubic boron nitride, to cemented carbide [2,3]. While few investigations using uncoated micro end mills were reported in literature [4,5], majority of the past works were carried out using coated tools. Although coating on the micro-mills undesirably increases the edge radius [6], coated tools outperform uncoated tool in several aspects.

To understand the evolution of tool wear during micro-milling, several investigations were carried out by different researchers. Ucun et al. (2013) [7] studied the performance of single-layer (DLC, TiAlN, and AlCrN) and multi-layer (TiAlN+AlCrN and TiAlN+WC/C) coatings on carbide substrate during micro-milling of Inconel 718. Low feed (1.25 μm/flute) showed excessive tool wear for all coating materials. Minimum Quantity Lubrication (MQL) significantly reduced wear rate and discouraged built-up edge formation as compared to dry cutting. During pocket milling on stainless steel using 800 μm tungsten carbide tools, Oliaei and Karpat (2016) [8] highlighted that tool wear predominantly evolve through edge rounding and flank wear. Worn-out tools tend to undergo transverse deflection opposite to the tool-feed direction, and as a consequence, each cutting edge in every rotation failed to remove

* Corresponding author:
E-mail address: ppb@mech.iitkgp.ac.in (P.P. Bandyopadhyay).

https://doi.org/10.1016/j.ijmecsci.2021.106844
Received 8 July 2021; Received in revised form 13 September 2021; Accepted 26 September 2021
Available online 2 October 2021

Nomenclature

N	Spindle speed (rotational speed of the tool) (rpm)
f_z	Feed per flute (μm/flute)
a_p	Axial depth of cut (μm)
V_C	Cutting velocity (μm/s)
V_F	Chip flow velocity (μm/s)
D_C	Outer diameter of the micro-end mills (μm)
r_e	Cutting edge radius (μm)
γ_O	Orthogonal rake angle of the tool (°)
α_O	Orthogonal clearance angle of the tool (°)
ψ	Helix angle of the tool (°)
γ_{avg}	Weighted average orthogonal rake angle of the entire rounded edge (°)
$\gamma_{avg}^{(shear)}$	Weighted average orthogonal rake angle at the shearing-dominant region (°)
a_1	Uncut chip thickness that is undergoing shearing (μm)
a_2	Measured thickness of the sheared chip (μm)
ζ	Chip reduction coefficient, CRC (also called chip thickness ratio, CTR)
$\Delta\zeta$	Difference in CTR value between dry and MQL micro-milling (%)
β_O	Orthogonal shear angle (°)
η	Friction angle at the chip-tool interface (°)
μ	Apparent coefficient of friction at the chip-tool interface
C	Machining constant at Merchant's Second Solution (°)
ε_e	Elastic strain of the workpiece material
θ_i	Instantaneous angular location of an edge during engagement period (°)
h_i	Instantaneous uncut chip thickness (μm)
h_{min}	Minimum uncut chip thickness for ploughing to shearing transition (μm)
h_{er}	Thickness of the elastically regained part on the micro-milled surface (μm)
y_i	Radial length of the tribo-contact region on the rake face (μm)
$L_{chip-tool}$	Tribo-contact length between the flowing chips and rake face (μm)
$L_{tool-wp}$	Tribo-contact length between the tool and the workpiece (μm)
T_{eng}, T_{dis}	Engagement and disengagement period between a particular cutting edge and the workpiece for every tool rotation (s)
$T_{chip-tool}$	Contact duration between the flowing chip and tool (s)
$T_{tool-wp}$	Contact duration between the workpiece and tool (s)
K_B	Face wear width (μm)
V_B	Flank wear length (μm)
F_X	Longitudinal force (N)
F_Y	Transverse force (N)
$F_{X,max}^{(shear)}$	Maximum longitudinal force arising owing to shearing only (N)
$F_{Y,max}^{(shear)}$	Maximum transverse force arising owing to shearing only (N)
$N_{max}^{(shear)}$	Maximum normal force arising owing to shearing only (N)
$F_{X,max}^{(Plough)}$	Maximum longitudinal force arising owing to ploughing only (N)
$F_{Y,max}^{(Plough)}$	Maximum transverse force arising owing to ploughing only (N)
$\sigma_{n,i}$	Instantaneous average normal stress (MPa)
σ_u	Ultimate tensile strength of the workpiece material (MPa)
τ_{ds}	Dynamic shear stress of the workpiece material (MPa)
$n_{shearing}$	Index for hyperbolic distribution of the stress in shearing region
$n_{ploughing}$	Index for hyperbolic distribution of the stress in ploughing region

material. Usage of higher feed per flute was suggested for efficient micro-milling with a worn out tool. During micro-milling of Inconel 718 using 300 μm diameter TiAlN-coated WC/6Co tools, Lu et al. (2016) [9] experimentally observed that tool wear initially proceeds through edge rounding where only edge radius can be measured. Tool matrix exposed only after about 2.0 minutes of machining making it feasible to measure flank wear length. Lu et al. (2017) [10] developed a cutting force prediction model for micro-milling with a flank-flattened tool; however, the condition for the onset of flank wear was not established. During dry micro-milling of pure titanium using TiAlN-coated WC tools, Miranda et al. (2018) [11] found that 50 μm axial depth of cut can be considered as optimum for reducing tool wear rate maintaining material removal adequately high for longer duration of cutting.

Jahan et al. (2019) [12] showed that TiAlN coating outperformed TiN coating in effectively reducing tool wear. Chip adhesion, edge chipping, and catastrophic breakage were found to be the primary modes of wear during micro-milling of polycarbonate. However, most of the adhered deposits were observed away from the active portion of the cutting edge, and thus, such adhesions are likely to have negligible impact on machining performance. While developing a protocol for micro-milling tool wear measurement, Alhadeff et al. (2019) [13] highlighted that the edge radius, face wear length, and flank wear length are three crucial parameters that can be quantitatively measured for assessing progressive tool wear. Dadgari et al. (2018) [14] identified three stages (rapid initial wear, gradual but non-uniform expansion of the wear land, and final accelerated wear) during experimental observation of the tool wear pattern in micro-milling of Ti-6Al-4V. For 1.0 mm diameter tool, 37.5 μm flank wear, 33.0 μm edge radius, or 1.0 μm average surface roughness was proposed as the tool failure criterion. Wear behaviour of 1.0 mm TiAlN coated WC tools during dry micro-milling of Ti-6Al-4V at a relatively low speed (5,000 rpm) was investigated by Vipindas and Mathew (2019) [15]. Tool edge radius gradually increased with the length of cut. Once the edge radius of the worn out tool exceeded feed per flute, material removal mechanism shifted from shearing to predominantly ploughing. Chip-adhesion, that was found prominent after 150 mm length of cut, aggravated the tool wear through chipping, coating delamination, and flank-flattening.

To explore the influences of tool wear on machinability during micro-milling of Ti-6Al-4V using $Ti(C_7N_3)$ based cermet tools, Wang et al. (2020) [16] briefly mentioned that adhesion, built-up edge formation, and micro-chipping were primary modes of tool wear. Although the effects of worn-out tool on machinability were studied, the progression of tool wear scenario was not discussed in details. Considering the micro-end milling tool wear as "stochastic", Zhang et al. (2020) [17] recorded 70 – 80 μm flank wear length on a 508 μm carbide cutter after 300 seconds of micro-milling. However, the progressive growth pattern of the flank wear was not analysed. Simultaneous wear of the rake surface and edge radius were also not taken into account. To study the wear behaviour of 152.4 μm TiAlN coated carbide tools during micro-milling of Ti-6Al-4V, Ziberov et al. (2020) [18] observed that the tool rapidly experienced 8 μm wear within 4.2 mm length of cut, and eventually expired the service-life (set to 15 μm wear length) within about 21 mm cut. Although edge chipping occurred within 8.4 mm cut, the tool survived without total breakage even up to 140 mm cut. Highlighting the difficulty in comprehending the pattern of tool wear, Varghese et al. (2021) [19] emphasized that edge chipping is the most dominant type of wear experienced by 500 μm diameter WC micro-mill during machining stainless steel. Edge radius was found preferred index for quantitative assessment of the tool wear in the initial stages; however, flank wear length was preferred index post-chipping.

In macro-scale machining, application of sustainable cooling-lubrication technique minimum quantity lubrication (MQL) showed positive results towards retarding tool wear rate [20]. Working with 200 μm diameter CrAlN-coated cemented carbide micro-mills, Silva et al. (2019) [21] highlighted that application of MQL can advantageously reduce the wear rate by 80 – 90% as compared to dry cutting. Khaliq et al. (2020) [22] experimentally investigated the benefits of MQL during slot milling on titanium alloy using TiAlN coated 500 μm WC tools. 40 – 50 μm reduction in tool diameter in dry cutting and 20 – 30 μm reduction in MQL cutting were recorded after 500 mm cut. Effects of MQL were more pronounced at lower speed (15,000 rpm). Various wear modes (edge rounding, chip-adhesion, delamination, chipping, flank wear) were observed by Anand Krishnan and Mathew (2020) [23] during micro-milling of Inconel 718 using AlTiN coated WC tools. Rapid wear occurred initially up to 30 mm length of cut, and thereafter gradual wear continued for another 120 – 210 mm cut before final breakage. A higher feed (6 μm/flute) exhibited 60% longer tool-life compared to a lower feed (0.5 μm/flute). Wang et al. (2020) [24] highlighted that MQL not only reduces the tool wear, surface roughness, feature inaccuracy, and cutting forces but also positively contributes in process stability, sustainability, and operator's health.

Tool wear has several detrimental effects on the overall micro-milling performance. With the progressive wear of the micro-milling tool, the cutting forces and surface roughness increase [25], system vibration increases [26], corner rounding of the milled feature increases [27], kerf width reduces [28], burr size increases [29], thickness of the plastically deformed subsurface layer expands [30], and nano-hardness of the milled surfaces decreases [31]. Higher edge radius is also associated with the generation of thicker chips [32] and incorporation of higher compressive residual stresses on the micro-milled surfaces [33]. Machining with a worn-out tool is also associated with higher specific energy consumption [34] that deviates the process from sustainable one [35]. Given the short life of the expensive micro-milling tools, it is essential to understand the mechanisms of various modes of tool wear for judicious selection of tool material and process parameters. Based on the above-discussed review of past works, following few gaps in literature can be identified for framing the objective.

It is well-known that the tool-wear rate in machining depends on a large number of factors including tool-workpiece material combination, inherent deformation mechanics, tribo-contact scenario, process parameters, lubrication, system condition, etc. However, in most of the past works in literature, conclusions were drawn mainly based on the experimental observations that limit the adaptability and applicability of the inferences. Underlaying mechanisms of various modes of micro-milling tool wear were also not systematically explored considering the cumulative effects of cutting mechanics, tool geometry, lubrication, and process parameters. Criteria for the onset of various modes of wear were also not explored. Progressive nature of the abrasion wear with the length of cut was given limited importance while studying other types of wear such as chip adhesion and edge-chipping.

Several researchers also attempted to understand the effects of sustainable MQL cooling-lubrication technique in controlling micro-milling tool wear; however, clearly contradictory observations were made. While several authors [21–23] inferred that the application of MQL can advantageously improve tool life, Ziberov et al. (2020) [18] experimentally found an opposite effect. In contrary to the general belief, application of MQL led to the reduction in tool-life as compared to dry cutting. Mechanisms of action of the cutting fluid in altering inherent material removal mechanics and controlling the tool wear rate were not studied in details. Analytical work in this aspect is thus necessary to understand the way cutting fluid can influence progressive wear.

There are also diverse observations on the edge-chipping scenario (most severe form of wear in micro-milling). Even dos Santos et al. (2018) [36] reported chipping within just 5 mm length of cut. It is thus pertinent to develop the conditions for edge-chipping, and understand the effect of parameters and tool-workpiece materials on it. In general, the edge-chipping and tool failure criteria are governed by the normal stresses acting on the tool [37]. However, no article in literature attempted to explore the form stability of the micro-milling tools through the variation of the normal stresses on the rounded cutting edges for a given set of conditions using the fundamental parameters. Accordingly, a holistic analysis of the progressive wear of the micro-milling tool is carried out in this article comprising the stress distribution, tool geometry, process mechanics, lubrication, and tribological aspects. The objectives of this investigation are listed below.

Table 1
Properties of the workpiece material

Property	Value
Material	Titanium alloy (Ti-6Al-4V)
α-phase composition (wt %)	92.40% Ti, 5.77% Al, 1.54% V
β-phase composition (wt %)	89.10% Ti, 3.93% Al, 6.77% V
Hardness	3.14 GPa
Tensile strength	860 MPa
Young's Modulus	115 GPa
Elongation	10%

- To assess the apparent co-efficient of friction at the chip-tool-workpiece interfaces in order to estimate the minimum uncut chip thickness during micro-milling under varying process parameters and lubrication conditions.
- To study the progressive wear scenario of micro end milling tools for distinguishing various stages, and to further explore underlaying mechanisms of various types of tool wear to draw recommendations for retarding wear rates.
- To analytically estimate and experimentally validate the face wear width and normal stresses acting on the tool considering the inherent mechanism of material removal, geometry of the rounded edge, cutting forces, and the progressive tool wear scenario.
- To study the mechanism of tool failure by edge chipping through the normal stress analysis with the progression of micro-milling.
- To explore the roles of MQL cutting fluid in altering the process mechanics and controlling the tool wear rate during micro-milling.

2. Experimental details

Ti-6Al-4V titanium alloy of size 20×20×10 mm^3 are chosen as workpiece material (Table 1). After mounting the as-received sample on the mechanical vice, facing of the top surface is carried out using a larger (5.0 mm) diameter end-milling cutter to ensure flatness of the top surface. An island of 5 mm width, 10 mm long and 3 mm height is also prepared on such samples (Fig. 1a-b). Without altering the gripping, micro-milling slots are machined on this island. A KERN-Evo ultra-precision CNC micro-machining centre (KERN microtechnik, Germany) is employed for micro-milling experiments. Straight micro-milling slots of 5 mm length (equals to the width of the island) with side-entry and side-exit of the tool are cut on the island with varying parametric conditions.

TiAlN-coated tungsten carbide end-mills (AXIS-Microtools, India) of 500 μm diameter are used for micro-milling of full-immersion slots (Fig. 1e-f). Crucial features of the tool are given in Table 2. Tool overhang length from the gripper is also attempted to keep constant across all the trials to eliminate variation in cutting dynamic effects [38]. As given in Table 3, spindle speed is varied in four intervals within the range 15,000 – 45,000 rpm that transforms to 23.6 – 70.7 m/min cutting velocity. To ensure chip shearing by each cutting edge in every tool rotation, the feed per flute is selected to a substantially higher value (4 μm). Axial depth of cut is also fixed to 50 μm. A fresh tool is assigned for each set of parametric condition; however, tool conditions are inspected

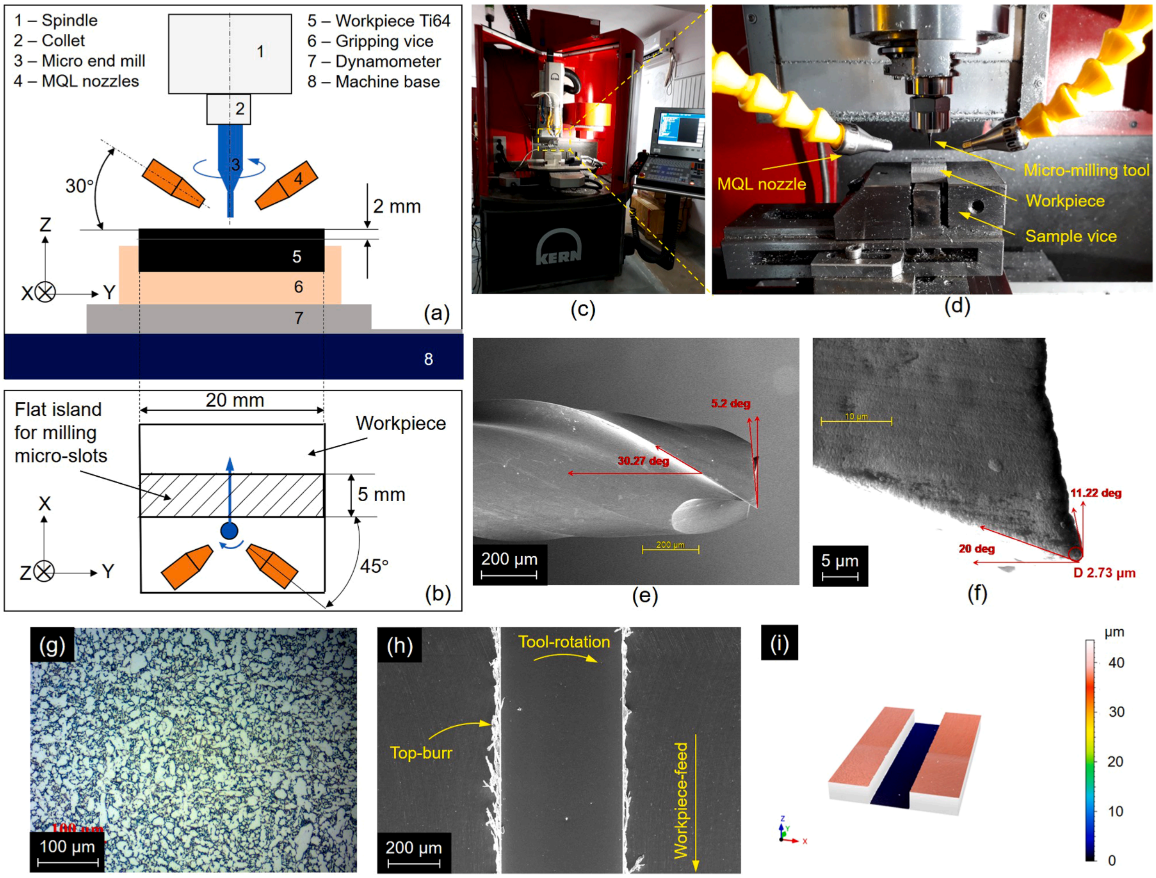

Fig. 1. Experimental details (a-b) schematic of the experimental set-up in side-view and top-view, (c-d) the KERN-Evo micro-milling machine with the enlarged view of the cutting zone, (e) side-view of the 0.5 mm diameter micro-end milling tool showing 30° helix angle and 5.2° bottom clearance angle, (f) cutting edge with 11.25° rake angle, 20° clearance angle, and 1.35 μm edge radius, (g) microstructure of the Ti-6Al-4V samples before micro-milling, (h) typical appearance of the micro-milling slot with protruded burrs on the side walls, and (i) typical 3D scanned profile of a micro-milled slot

Table 2
Features of the two-flute flat-end micro end milling tool

Property	Value
Cutter diameter	0.5 mm
Helix angle	30°
Axial (orthogonal) rake angle (γ_O)	11.25±0.41°
Axial (orthogonal) clearance angle (α_O)	20±0.36°
Edge radius (r_e)	1.3±0.09 μm
Substrate material	WC/6Co
Substrate composition (wt%)	39.67% W, 51.77% C, 5.45% Co
Coating material	TiAlN
Coating composition (wt%)	38.68% Ti, 29.76% Al, 31.56% N
Coating thickness at rounded edge	1.5 – 2.5 μm

Table 3
Fixed and variable process parameters set during experimentation

Parameter	Value
Rotational speed (N)	15000, 25000, 35000, 45000 rpm
Table feed (f_z)	4.0 μm/flute
Axial depth of cut (a_p)	50 μm
Lubrication	Dry, MQL

after every 5 mm length of cut.

The entire set of experiment is performed in two different cutting environments (dry and MQL). While the dry cutting is carried out without any additional cutting fluid, an eco-friendly (biodegradable) commercial cutting oil UNILUBE 2032 (UNILUBE AG, Switzerland) at 6 mL/h flow rate is delivered into the machining zone during MQL based sustainable micro-milling. The micro-milling machine, used for this experimentation, is fitted with an ECOLUBE-2D fluid delivery system that can dispense very fine oil droplets of average diameter 5 – 10 μm. Two nozzles are directed to the cutting zone in such a fashion (Fig. 1a-b) that it can deposit oil droplets directly on the trailing edge during the disengagement period. Following the recommendation of Vazquez et al. (2015) [39], the MQL nozzles in X-Y plane are placed behind the tool at 45° angle with the feed direction maintaining uniformity in up-milling (conventional milling) and down-milling (climb milling) sides.

A multicomponent piezoelectric dynamometer (9119AA2, KISTLER) is engaged for sensing real time force signals in three mutually perpendicular directions. Force components along the feed direction, perpendicular to the feed direction and along the tool axis are termed as longitudinal force (F_X), transverse force (F_Y) and axial force (F_Z), respectively. Three charge amplifiers (5015, KISTLER) and a digital storage oscilloscope (DSO-X 2014A, Agilent InfiniiVision) are also employed for gathering quantitative force data, which are further processed in MATLAB software for retrieving desired force values. Chips that are generated during micro-milling are also collected using double sided conductive adhesive carbon tape, and the same are observed under a Scanning Electron Microscope (SEM) (EVO 18, ZEISS, Germany). Such SEM images are further analysed using compatible AxioVision software. Condition of the tool after every 5 mm length of cut is also observed under the same SEM and quantitatively analysed further. This SEM is fitted with an energy-dispersive X-ray spectroscopy (EDS) facility that is also used for evaluating elemental compositions. To observe microstructure of the post-milled Ti-6Al-4V samples, the micro-milled slots

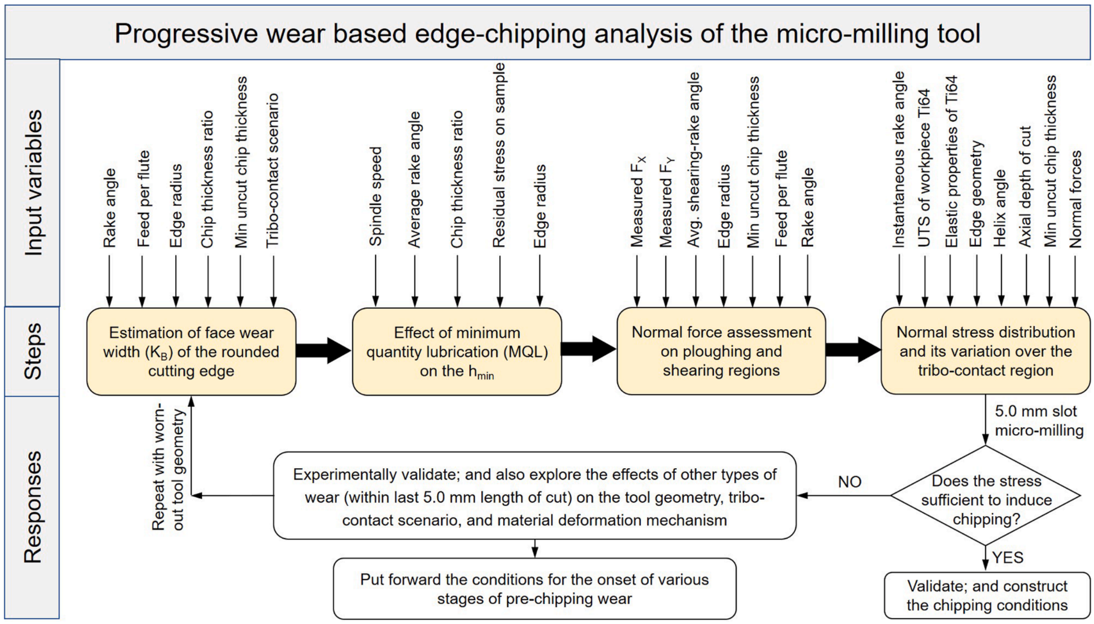

Fig. 2. Flow diagram that displays the sequences along with the input variables that are followed for the analytical development of the edge-chipping criteria with the progressive wear of the micro-milling tool

are sliced along the transverse direction using wire-electric discharge machining (W-EDM). The sliced samples are then successively polished and swab-etched using Kroll's reagent (mixture of 92 ml distilled water, 6 ml nitric acid, and 2 ml hydrofluoric acid) before observing under the microscope.

3. Analytical modelling

In general, macro cutting tool fails through catastrophic breakage, rapid dulling, and/or gradual wear. Among these three common ways, rapid dulling and few thermo-chemical wear modes are highly sensitive to cutting temperature. In micro-milling, the cutting zone temperature remains considerably low, typically around 60 – 80°C [40]. Neglecting the chances of thermally activated tool-failure modes, attention can therefore be concentrated on the mechanical wears and catastrophic failure of the micro-milling tools for modelling purpose. As shown through the flow diagram of Fig. 2, an analytical model is first developed to estimate the face wear width using the tribological contact scenario between the chip-tool-workpiece. The effects of minimum quantity lubrication (MQL) on controlling the material deformation scenario is thereafter assessed. Based on the measured force components, the normal forces acting on the ploughing-dominant and shearing-dominant regions are estimated. Intensity and variation of the normal stresses on the rounded cutting edge are further analysed and tallied with the properties of the tribo-pair to understand possible wear scenario. Various stages of wear are characterized, and the conditions for their

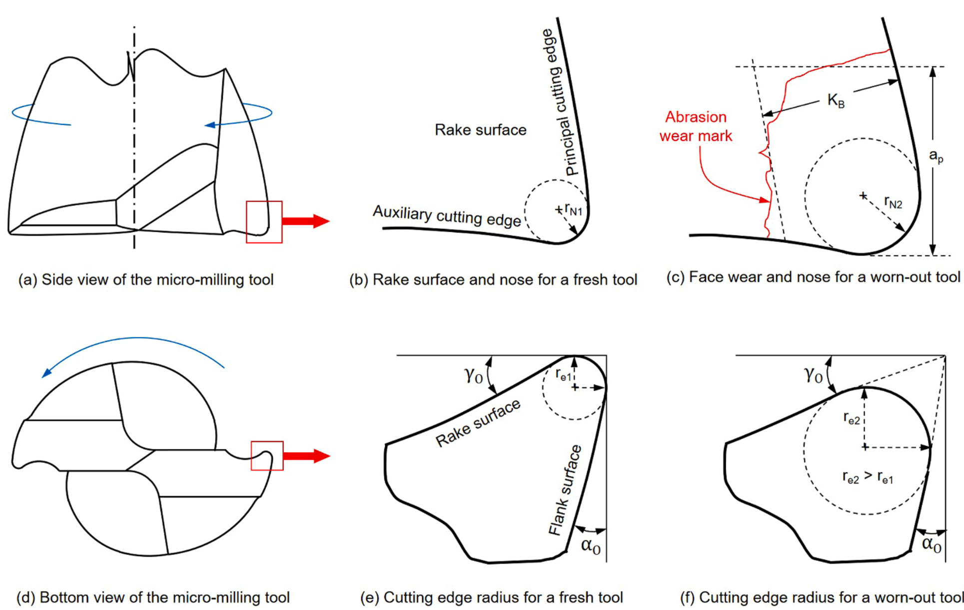

Fig. 3. Schematic representation of the (a-b) side view and bottom view of the two-flute flat-bottom helical micro-milling tool, (c-d) enlarged tool-nose and cutting-edge in the fresh condition showing the nose radius and edge radius, (e) development of abrasion mark on the rake surface when used for machining, and (f) increase in edge radius owing to tool wear

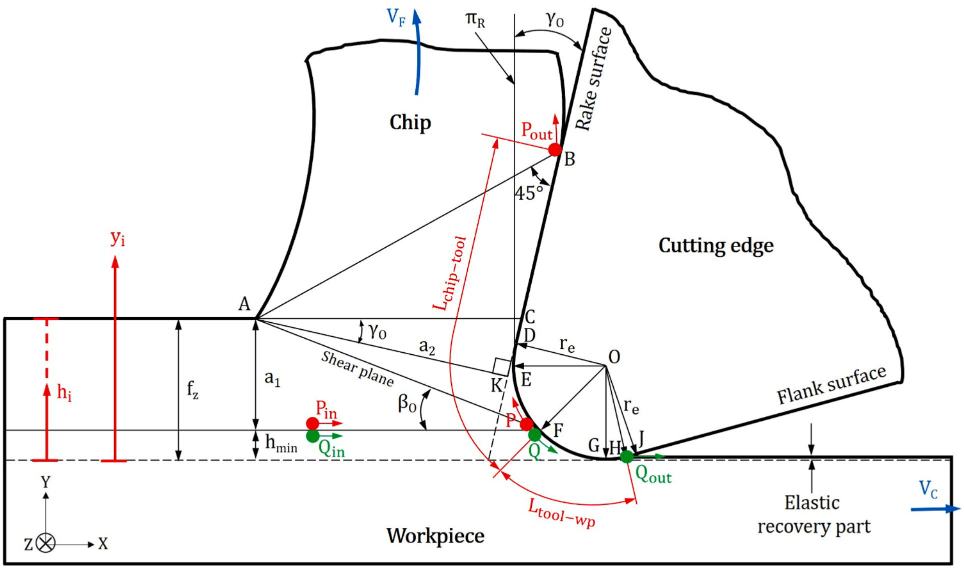

Fig. 4. Schematic representation of the chip-tool-workpiece tribo-contact scenario on the orthogonal plane for maximum uncut chip thickness ($h_i = f_z$) condition at 90° immersion angle for substantially higher feed per flute value as compared to the edge radius ($f_z > r_e$). Of the total f_z uncut chip thickness, material of h_{min} thickness undergoes ploughing, while rest of the material undergoes shearing to produce chips. The flowing chip maintains plastic contact with the rake surface up to point-B, while the machined surface leaves the flank face at point-H. (Laterally deformed material or burr is not shown here)

onset are analytically developed. The progressively worn-out tools are re-used until edge-chipping. The benefits and drawbacks of the application of MQL on micro-milling tool wear are further highlighted.

3.1. Fundamental considerations for the assessment of micro-milling tool wear

When a fresh micro-end mill is engaged in machining, its rounded cutting edge with a small portion (1 – 4 µm) of rake and flank surfaces actively participate in material removal. However, when chip flows over the rake surface, the tribo-contact region expands over a relatively larger area beyond the tool edge. Face wear width (K_B) is the measure of the average width of such tribologically active portion on rake surface that is susceptible to loss of material during machining (Fig. 3). As the micro-milling progresses, the entire rounded edge undergoes gradual loss and/or adherence of material, and thus, the edge geometry changes with the length of cut. Accordingly, an analysis purely based on a fresh tool fails to provide reliable estimations of the face wear and form stability of the edge. The progression of the tool wear through different stages must be inclusively considered for tool failure analysis. Based on the following assumptions, analytical estimations of face wear length, effects of MQL lubrication, and stress distribution are first carried out for a fresh tool, and the same are extended to a worn-out tool.

- Cutting action takes place in a very small region (15 – 20 µm) at the tool-tip, and thus, the rake surface and flank surface beyond the rounded-edge can be considered as flat surfaces. So the tool has a constant rake angle and clearance angle outside the rounded-edge.
- As the nose radius is significantly smaller than the axial depth of cut, the effects of the variation of the nose radius with the length of cut is neglected.
- Feed per flute is adequately higher than the edge radius of the fresh tool.

3.2. Chip-tool-workpiece tribo-contact scenario

Micro-end milling is inherently an intermittent cutting process where each cutting edge engages and disengages with the workpiece in every tool rotation. In full-immersion milling, the contact between a particular cutting edge and workpiece occurs for 180° tool rotation, while the same cutting edge remains disengaged for rest half of the rotation. When a micro end milling tool of diameter D_C (mm) rotates at N (rpm), the engagement period (second) between a cutting edge and the workpiece for one tool rotation can be expressed through Eq. (1). The engagement period (T_{eng}) and disengagement period (T_{dis}) are equal for full-immersion milling, and both are independent of the number of cutting edges present on the cutter body.

$$T_{eng} = T_{dis} = \frac{60}{2N} \tag{1}$$

During the engagement period, the uncut chip thickness does not remain constant. The instantaneous uncut chip thickness (h_i) increases from zero to maximum at the end of up-milling quarter-circle, and again decreases from maximum to zero at the end of down-milling quarter-circle. In absence of tool deflection (run out), the maximum uncut chip thickness is equal to the feed per flute (f_z). It is now well-established fact that the workpiece material fails to undergo smooth shearing until the uncut chip thickness reaches a critical value (called minimum uncut chip thickness, h_{min}). For $h_i \le h_{min}$, a strip of workpiece material of thickness h_i undergoes elastic-plastic deformation (ploughing). For $h_i > h_{min}$, a thin strip of workpiece material having thickness h_{min} undergoes ploughing, while rest of the material ($h_i - h_{min}$) undergoes shearing to produce chips (Fig. 4). For the sake of modelling, it is assumed that ploughing to shearing transition occurs along a thin 2-D plane located at $h_i = h_{min}$.

The chip-tool-workpiece tribo-contact scenario for maximum uncut chip thickness condition ($h_i = f_z$) is shown in Fig. 4. As usual, workpiece material of thickness ($f_z - h_{min}$) experienced shearing to produce chip of thickness a_2. Based on Lee and Shaffer's slip-line theory, boundary of the plastic zone is assumed to meet the rake surface at 45° angle [41]. For modelling purpose, dead metal zone formation [42] ahead of the cutting edge is neglected. Consider an element of workpiece material at an arbitrary point-P located just above h_{min}, and another elemental point-Q just below h_{min}. Both these elements are initially a part of the workpiece and move at same velocity V_C. The element-P experiences shear deformation at point-F to become an integrated part of the chip. This element then moves a distance $L_{chip-tool}$ at a velocity V_F before plastically separating from the rake face at point-B. Corresponding tribo-contact length ($L_{chip-tool}$) can be calculated geometrically, as deduced below.

$$BC = (BK - CK) = a_2(1 - \tan\gamma_O)$$

$$CD = \frac{f_z - r_e - r_e\sin\gamma_O}{\cos\gamma_O} = \frac{f_z - r_e(1 + \sin\gamma_O)}{\cos\gamma_O}$$

$$DE = r_e\left(\frac{\pi\gamma_O}{180}\right)$$

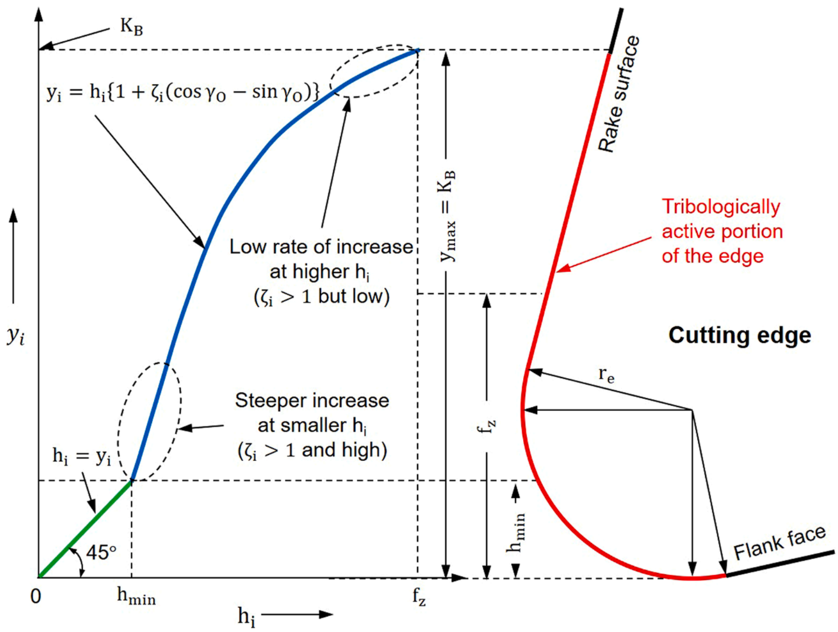

Fig. 5. Typically shows the variation of the tribo-contact length (y_i) on the rake face for the variation in uncut chip thickness (h_i). The y_i initially increases proportionally as h_i increases within the ploughing-dominant region (i.e. up to $h_i = h_{min}$). However, y_i increases steeply with the further increase in h_i within the shearing-dominant region owing to chip formation, and corresponding the rate of increase depends on the value of chip thickness ratio (ζ). This ζ is usually higher for the lower values of uncut shear-able chip thickness

$$EF = \frac{\pi r_e}{180}\sin^{-1}\left(1 - \frac{h_{min}}{r_e}\right)$$

$$\therefore L_{chip-tool} = a_2(1 - \tan\gamma_O) + \frac{f_z - r_e(1 + \sin\gamma_O)}{\cos\gamma_O} + r_e\left(\frac{\pi\gamma_O}{180}\right) + \frac{\pi r_e}{180}\sin^{-1}\left(1 - \frac{h_{min}}{r_e}\right) \tag{2}$$

The average velocity of this element-P is same with the average flow velocity of the chip (V_F). The V_F can be obtained by equating volumetric flow rate of the material before and after shearing. Considering no lateral flow of the material within $h_{min} < h_i \le f_z$, the V_F can be expressed in terms of cutting velocity (V_C) or spindle speed (N) in the following form.

$$V_F = \left(\frac{f_z - h_{min}}{a_2}\right)V_C = \frac{1000\pi D_C N(f_z - h_{min})}{60a_2} \tag{3}$$

On the other hand, the element-Q experiences elastic-plastic deformation at point-F. The plastically deformed material flows in lateral direction, while the elastically deformed part regains its shape to become a part of the final surface once the tool moves past it. The tribo-contact between the cutting edge and the workpiece remains equal to the arc length F-G-H. To obtain the tribo-contact length, height of the elastic regain part (h_{er}) is required to calculate. For a given workpiece material with known elastic strain (ε_e), the h_{er} can be expressed as follows.

$$h_{er} = \varepsilon_e h_{min} \tag{4}$$

Therefore, the tribo-contact length ($L_{tool-wp}$) between the tool and workpiece can be calculated geometrically and expressed in the following form. The average relative velocity between tool-workpiece pair is same with the cutting velocity (V_C).

$$L_{tool-wp} = \frac{\pi r_e}{180}\left\{\cos^{-1}\left(1 - \frac{h_{min}}{r_e}\right) + \cos^{-1}\left(1 - \frac{h_{er}}{r_e}\right)\right\} \tag{5}$$

3.3. Estimation of face wear width in a measurable form

The intended face wear width can be apparently obtained using Eq. (2). However, $L_{chip-tool}$ is a function of chip thickness (a_2). Measurement of chip thickness for all the trials is a cumbersome task. Furthermore, as the edge radius changes with the progression of micro-milling, the minimum uncut chip thickness (h_{min}) changes proportionally. Accordingly, the uncut chip thickness ($f_z - h_{min}$) changes with the length of cut even when the feed per flute is constant. Different lubrication conditions and parameters can also alter the h_{min} value. Since the chip thickness (a_2) does not vary linearly with the uncut chip thickness (a_1), a parameter called chip thickness ratio (ζ) is introduced that is defined by the ratio between chip thickness and uncut chip thickness.

$$\zeta_i = \frac{a_{2,i}}{a_{1,i}} \tag{6}$$

Expression of ζ_i as a function of uncut chip thickness can be developed through a small number of experiments, and the same can be used to estimate the chip thickness for a known value of ($f_z - h_{min}$). Additionally, minimum uncut chip thickness (h_{min}) estimation for different conditions is also a necessity.

As shown earlier in Fig. 3c, SEM based measurement of K_B is carried out by observing the rake surface of the tool on the axial plane. On such a projected view, the inclined lengths as utilized in Eq. (2) cannot be measured. Instead, a projected length parallel to h_i (Fig. 4) between the tool-tip and point-B can be measured. As the parameter h_i is defined with the upper limit of f_z ($0 < h_i \le f_z$), a new reference axis (y) is required to introduce here. The y_i $\left(0 \le y_i < \frac{D_C}{2}\right)$ indicates the radial distance of the last plastic-contact point between chip-tool on the rake surface from the tool-tip. The relation between h_i and y_i depends on the region of analysis, as discussed below.

Within the ploughing dominant region ($0 \le h_i \le h_{min}$), the height of the tribo-contact portion increases equally as uncut chip thickness increases. Therefore, $h_i = y_i$ for $0 \le h_i \le h_{min}$. As h_i increases beyond h_{min} ($h_{min} < h_i \le f_z$), chip formation begins and the tribo-contact shifts from tool-workpiece to chip-tool. In this shearing-dominant region, the length y_i not only depends on h_i but also changes with the ζ_i based on the ($f_z - h_{min}$) value. Variation of y_i with h_i in ploughing-dominant and shearing-dominant regions is also shown in Fig. 5. The corresponding relation between y_i with h_i for $h_i > h_{min}$ can be established geometrically from Fig. 4, and expressed in the form of Eq. (7). Note that ζ_i is always greater than 1.0; however, its value is more at lower uncut chip thickness. Thus the rate of increase of y_i with h_i in the shearing-dominant region gradually reduces with an increase in uncut chip thickness.

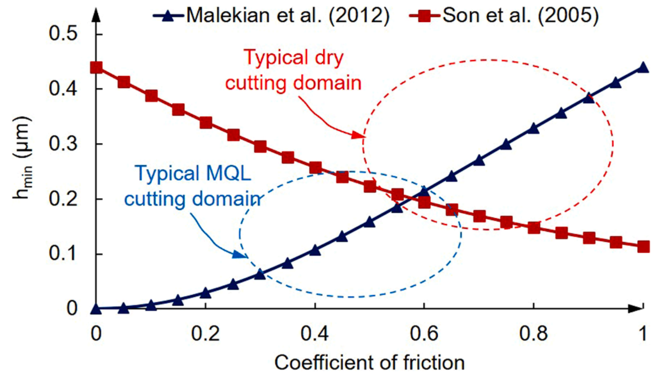

Fig. 6. Dependency of minimum uncut chip thickness (h_{min}) on the coefficient of friction (μ) at the chip-tool-workpiece interfaces as proposed by different researchers (typically shown for an edge radius of 1.5 μm). According to Son et al. (2005), h_{min} is inversely proportional to μ, and thus higher h_{min} is expected in MQL assisted cutting as compared to that of dry cutting. On the contrary, a proportional relationship was proposed by Malekian et al. (2012) that gives lower h_{min} value in MQL based cutting as compared to that of dry cutting

$$y_i = h_i + CB\cos\gamma_O = h_i\{1 + \zeta_i(\cos\gamma_O - \sin\gamma_O)\} \tag{7}$$

Note that the Eq. (7) can be used so long as $f_z > h_{min}$ condition is satisfied. With the progression of tool wear when the theoretical value of minimum uncut chip thickness (h_{min}) exceeds the set feed per flute, this equation fails to fetch reliable result. However, such a situation occurs at a very high value of edge radius. Several other phenomena (like chip-adhesion, non-cutting passes, etc.) occur before h_{min} reaches close to f_z. These factors that significantly alter the tribo-contact scenario are discussed in section-4. Thus, the K_B length can be expressed in the following form.

$$K_B = f_z\{1 + \zeta(\cos\gamma_O - \sin\gamma_O)\} \tag{8}$$

3.4. Assessment of the influence of minimum quantity lubrication (MQL)

One way of looking into the effect of MQL application is through its capability in reducing the minimum uncut chip thickness (h_{min}). In an early investigation, Son et al. (2005) [43] established an expression (Eq. 9) for h_{min} using the friction angle (η) between the tool and the sheared-chip. The dynamic coefficient of friction at the chip-tool interface (μ) is proportional to this friction angle (μ = tanη). Therefore, according to the Eq. (9), the h_{min} value increases when friction angle reduces or lubricant is applied (Fig. 6). This is less likely to occur as lower friction at the interface encourages chip formation by reducing the extent of ploughing.

$$h_{min} = r_e\left\{1 - \cos\left(\frac{\pi}{4} - \frac{\eta}{2}\right)\right\} \tag{9}$$

In an experimental investigation, a proportional relationship between the minimum uncut chip thickness (h_{min}) and friction coefficient (μ) was observed by Rezaei et al. (2018) [44] during dry and MQL assisted sustainable micro-milling of Ti-6Al-4V. While in dry cutting the h_{min} value existed in between 25–49% of the edge radius, the same decreased to 15–34% of the edge radius in MQL cutting. Malekian et al. (2012) [45] also put forward a relationship (Eq. 10) between h_{min} and friction angle using the minimum energy principle. According to Eq. (10), the h_{min} value reduces when coefficient of friction is reduced (or lubricant is applied), which is in line with the observations of Rezaei et al. (2018). Thus Eq. (10) is used in this investigation for analytical modelling.

$$h_{min} = r_e\{1 - \cos\eta\} \tag{10}$$

For the sake of modelling, here it is assumed that the apparent coefficient of friction remains unchanged over the entire chip-tool-workpiece contact region. However, μ can vary with the process parameters and cutting environment. Applying Merchant's Second Solution for minimum energy requirement for shearing along the concentrated shear plane [46], the average friction angle between the chip and the rake surface can be obtained through Eq. (11).

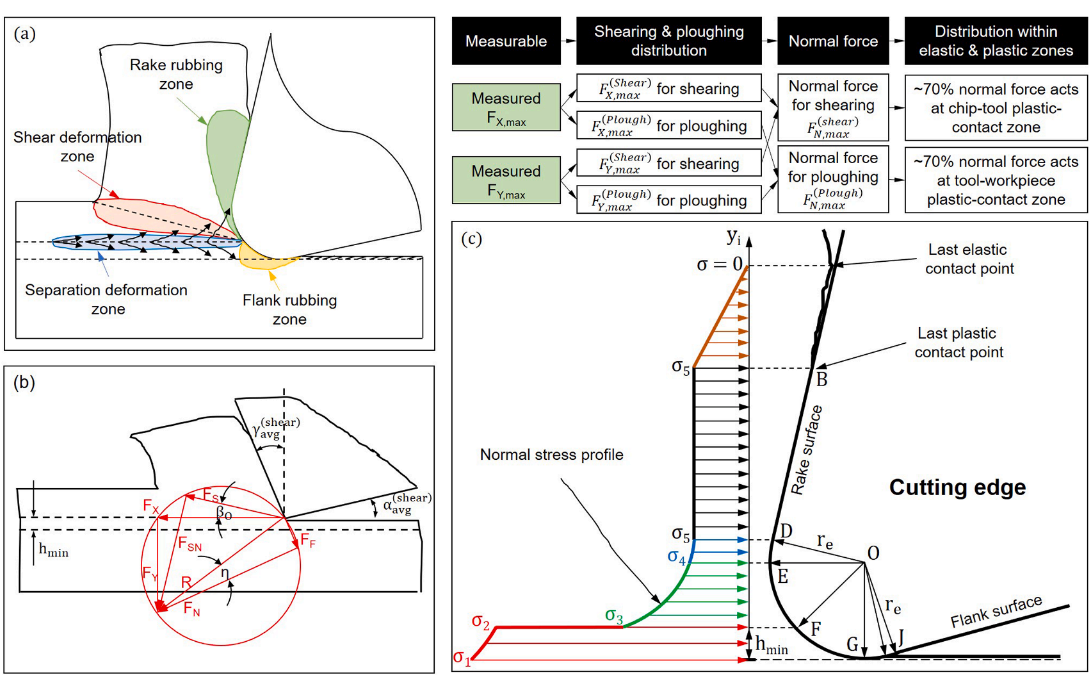

Fig. 7. Cutting force and normal stress analysis (a) representation of four deformation zones associated with micro-milling using a rounded edge tool, (b) Merchant's Circle Diagram (MCD) drawn based on the equivalent sharp tool within the shear dominant region showing different force components, (c) normal stress distribution profile on the cutting edge across the ploughing and shearing dominant regions (a flow chart to retrieve normal force on chip-tool and tool-workpiece interfaces from the measurable force components is also shown)

$$\eta = C + \gamma_{avg} - 2\beta_O \tag{11}$$

Where C is the machining constant, and its value relies on tool-workpiece material pair. This C value for harder engineering alloys mostly remains in between 85° – 92°. Cold working of the workpiece increases the C value. In this experimentation, facing is performed on the Ti-6Al-4V samples prior to micro-milling of slots that leads to the incorporation of compressive residual stress on the surface. Residual stresses of the pre-micromilled sample surface are measured following multiple exposure ($\sin^2\psi$) technique using X-Ray Diffraction system (PANalytical EMPYREAN) operated on copper anode source at 45 kV and 40 mA. For Ti-6Al-4V samples with 2θ peak position close to 141.645°, a scanning range of 139.645° – 143.645° is selected with a step size of 0.141 μm. Three repetitions are taken, and the average normal residual stress is found to be around –330 MPa (compressive). Such a high compressive residual stress produces similar effect to that of the cold working (strain hardening). Thus, in this work, C is assumed to be 90°. Furthermore, the rake angle over the chip-tool-workpiece is also not constant, and thus, a weighted average orthogonal rake angle (γ_{avg}) is estimated using the cutting edge geometry (Fig. 4).

$$\gamma_{avg} = \frac{GE\dfrac{\int_{\gamma_i=\gamma_G}^{\gamma_i=\gamma_E}(\gamma_i r_e)d\gamma_i}{\int_{\gamma_G}^{\gamma_E}(r_e)d\gamma_i} + ED\dfrac{\int_{\gamma_E}^{\gamma_D}(\gamma_i r_e)d\gamma_i}{\int_{\gamma_E}^{\gamma_D}(r_e)d\gamma_i} + DC(\gamma_O)}{GE+ED+DC} = \frac{-\dfrac{90\pi r_e}{4} + \dfrac{r_e(\gamma_O)^2}{2} + \dfrac{\{f_z - r_e(1+\sin\gamma_O)\}\gamma_O}{\cos\gamma_O}}{\dfrac{\pi r_e}{2} + (\gamma_O r_e) + \dfrac{f_z - r_e(1+\sin\gamma_O)}{\cos\gamma_O}} \tag{12}$$

$$\gamma_{avg}^{(shear)} = \frac{FE\dfrac{\int_{\gamma_i=\gamma_F}^{\gamma_i=\gamma_E}(r_e\gamma_i)d\gamma_i}{\int_{\gamma_F}^{\gamma_E}(r_e)d\gamma_i} + ED\dfrac{\int_{\gamma_E}^{\gamma_D}(r_e\gamma_i)d\gamma_i}{\int_{\gamma_E}^{\gamma_D}(r_e)d\gamma_i} + DC(\gamma_O)}{FE+ED+DC} = \frac{-\dfrac{\pi r_e}{2}\left\{\dfrac{1}{2} - \dfrac{1}{180}\cos^{-1}\left(1-\dfrac{h_{min}}{r_e}\right)\right\}\sin^{-1}\left(1-\dfrac{h_{min}}{r_e}\right) + \dfrac{\pi r_e}{2}\dfrac{(\gamma_O)^2}{180} + \dfrac{\{f_z - r_e(1+\sin\gamma_O)\}\gamma_O}{\cos\gamma_O}}{\pi r_e\left\{\dfrac{1}{2} - \dfrac{1}{180}\cos^{-1}\left(1-\dfrac{h_{min}}{r_e}\right)\right\} + \dfrac{\pi r_e \gamma_O}{180} + \dfrac{\{f_z - r_e(1+\sin\gamma_O)\}}{\cos\gamma_O}} \tag{14}$$

In Eq. (11), β_O is the average shear angle that can also be calculated using γ_{avg} and the chip thickness ratio (ζ) value using Eq. (13). Roles of MQL cutting fluid in altering h_{min} value under different parametric conditions are discussed in section-4.2.

$$\beta_O = \tan^{-1}\left(\frac{\cos\gamma_{avg}}{\zeta - \sin\gamma_{avg}}\right) \tag{13}$$

3.5. Estimation of the normal stresses acting on the cutting tool

In conventional machining with a sharp tool, the workpiece material first experiences shear deformation at the shear-zone to transform into chip after thickening. In micro-milling with a rounded tool, the workpiece experiences additional tearing prior to entering into the shearing zone. As shown in Fig. 7a, the very first deformation (tearing) occurs surrounding the minimum uncut chip thickness (h_{min}) line. This region is referred to as "Separation Deformation Zone" where the plough-able material separates from the shear-able material. Such separation actually occurs over a narrow region across the h_{min} line; however, here it is assumed to occur along a concentrated plane located at $h_i = h_{min}$. The shear-able material further undergoes shearing at the shear deformation zone to produce chip that again flows over the rake surface through the rake rubbing zone. On the other hand, a part of the plough-able material flows over the rounded edge and flank surface leading to the generation of flank rubbing zone.

To understand the normal stress variation over the contact length, the normal force exerted by the chip or workpiece on the tool needs to be estimated. The maximum values of the two measurable force components (longitudinal force F_X and transverse force F_Y) for one engagement between cutting edge and workpiece can be easily retrieved by analysing the dynamometer data. Using these maximum force values, Merchant's Circle Diagram (MCD) can be drawn to assess normal force. However, the layer of workpiece material within $0 \le h_i \le h_{min}$ undergoes elastic-plastic deformation, and a major fraction of this material flows in the lateral direction to produce burr [47]. This violets the plain strain condition for drawing MCD in this region [48]. The workpiece material within $h_{min} < h_i \le f_z$ undergoes shearing to produce micro-chips, and thus, MCD can be drawn only for this range of h_i.

Moreover, the average orthogonal rake angle (γ_{avg}) of the entire cutting edge is also not valid for this shearing-dominant region as γ_{avg} was calculated for the whole uncut chip thickness $0 < h_i \le f_z$ (Eq. 12). Thus, the weighted average orthogonal rake angle in shearing-dominant region $\gamma_{avg}^{(shear)}$ can be considered for further analysis using MCD. This angle $\gamma_{avg}^{(shear)}$ can be expressed in the form of Eq. (14) with the help of Fig. 4. Its value depends on the minimum uncut chip thickness, and thus, material deformation scenario with the variation of minimum uncut chip thickness (h_{min}) can be captured properly by using this equation.

Furthermore, the ploughing forces originating from ploughing-dominant region are subsumed within the measured forces. A flow chart to distinguish ploughing and shearing normal forces is shown in Fig. 7. Working with Ti-6Al-4V samples with 50 μm axial depth, Singh et al. (2015) [4] explored the variation of ploughing and shearing forces for different feed values. For f_z = 4 μm/flute, net force originating from shearing was found to be about 61% of the total force when critical uncut chip thickness was about 2.82 μm. However, as the minimum uncut chip thickness (h_{min}) varies, such contributions of the ploughing and shearing forces change. Therefore, for a finite value of h_{min}, the force components arising owing to shearing can be approximately estimated from the measured forces using the following equations.

$$F_{X,max}^{(Shear)} = \left(\frac{0.61}{4-2.82}\right)\left(\frac{f_z - h_{min}}{f_z}\right)F_{X,max} = 0.52\left(1-\frac{h_{min}}{f_z}\right)F_{X,max} \tag{15a}$$

$$F_{Y,max}^{(Shear)} = \left(\frac{0.61}{4-2.82}\right)\left(\frac{f_z - h_{min}}{f_z}\right)F_{Y,max} = 0.52\left(1-\frac{h_{min}}{f_z}\right)F_{Y,max} \tag{15b}$$

Using angular relationship from MCD (Fig. 7b), the net normal force (F_N) acting at the chip-tool interface within the shearing-dominant

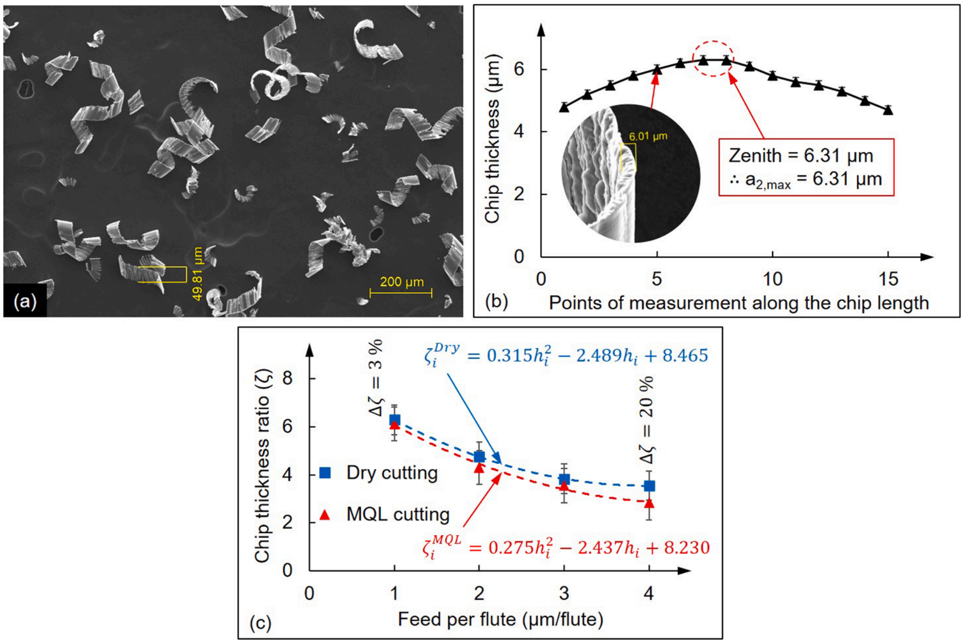

Fig. 8. Chip thickness measurement and its variation: (a) SEM image of the micro-chips collected simply by placing an adhesive carbon tape at the vicinity of machining zone during micro-milling experiments where continuous chip with favourable orientation can be used for measurement of chip thickness, (b) typical convex-shaped curve plotted from SEM-based thickness measurement data for obtaining maximum chip thickness for 25,000 rpm speed, 1.0 μm/flute feed, and 50 μm axial depth, and (b) variation of the chip thickness ratio with the feed per flute (or uncut chip thickness) for dry and MQL cutting

region can be calculated using Eq. (16).

$$F_{N,max}^{(shear)} = F_{X,max}^{(Shear)} \cos\gamma_{avg}^{(shear)} - F_{Y,max}^{(Shear)} \sin\gamma_{avg}^{(shear)} \tag{16}$$

Such MCD based analysis cannot be extended to the ploughing-dominant region. The force arising owing to ploughing (Eq. 17) can be calculated by subtracting the shearing-components from the measured ones. A factor $C_T = 0.6$ is also introduced to consider 40% of the remaining forces contribute to tearing failure of the workpiece material at the separation deformation zone. An average normal force equal to the resultant of the $F_{X,max}^{(Plough)}$ and $F_{Y,max}^{(Plough)}$ is assumed to act within the ploughing-dominant region (Eq. 18).

$$F_{X,max}^{(Plough)} = C_T\left\{F_{X,max} - F_{X,max}^{(Shear)}\right\} \tag{17a}$$

$$F_{Y,max}^{(Plough)} = C_T\left\{F_{Y,max} - F_{Y,max}^{(Shear)}\right\} \tag{17b}$$

$$F_{N,max}^{(Plough)} = \sqrt{\left(F_{X,max}^{(Plough)}\right)^2 + \left(F_{Y,max}^{(Plough)}\right)^2} \tag{18}$$

With the knowledge of the cutting forces, distribution of the normal stresses on the cutting edge can be assessed. Wang et al. (2019) [49] attempted to evaluate the tribo-contact stresses (pressures) to understand the fatigue failure behaviour of micro-milling tool; however, corresponding variation owing to the ploughing and shearing material removal mechanisms was not clearly distinguished. Detailed work focusing on the variation of normal stress around a rounded-edge cutting tool is not available in literature. However, it is well-known fact that a higher negative rake angle is associated with the higher degree of deformation of the workpiece material. Thus, the normal force acting at the chip-tool interface also rises as the rake angle increases towards more negative [50]. Assuming a hyperbolic distribution (index-n) of the normal stress at the plastic-contact region on chip-tool interface, the average normal stress (σ_n) variation can be expressed in the following manner as a function of instantaneous rake angle (γ_i) [51].

$$\sigma_{n,i} = \frac{2\tau_{ds}(1.285 - \gamma_i)}{n+1} \tag{19}$$

Where τ_{ds} is the dynamic shear stress that can be obtained from Abuladze's relationship (Eq. 20) using the known values of ultimate tensile strength (σ_u) and percentage elastic elongation (ε_e) of the concerned workpiece material [52].

$$\tau_{ds} = 0.74\sigma_u\left(6^{0.6\varepsilon_e}\right) \tag{20}$$

Normal stress also varies as the instantaneous rake angle changes. Eq. (21) gives the expressions of such variation for different segments of the cutting edge. Note that the standard sign convention for the positive and negative rake angle is also considered. A typical variation of the normal stress distribution on the tool is also shown in Fig. 7c. The stress is maximum at the tool-tip, and the same gradually decreases with the radially inward distance (y_i) as the rake angle becomes less negative. At the last point of the chip-tool plastic-contact zone (Point-B in Fig. 4), a finite normal stress acts on the tool. This stress gradually reaches to zero at the end of chip-tool elastic-contact zone. Normal stress is constant for the straight portion of the rake surface. Although the normal stress variation pattern is governed by Eq. (21), its magnitude for various process parameters and lubrications is guided by the index-n, as discussed below.

$$\sigma_{n,i} = \begin{cases} \dfrac{2\tau_{ds}}{n+1}\left\{1.285 + \sin^{-1}\left(1 - \dfrac{y_i}{r_e}\right)\right\}, & \text{for } 0 \le y_i \le r_e \\ \dfrac{2\tau_{ds}}{n+1}\left\{1.285 - \sin^{-1}\left(\dfrac{y_i}{r_e} - 1\right)\right\}, & \text{for } r_e < y_i \le r_e \sin\gamma_O \\ \dfrac{2\tau_{ds}}{n+1}\left\{1.285 - \gamma_O\right\}, & \text{for } y_i \ge r_e \sin\gamma_O \end{cases} \tag{21}$$

The index-n can be calculated through the force balance. Apart from lubrication condition, index-n also varies between the shearing-region and ploughing-region because ploughing requires higher specific energy as compared to shearing [53]. Force balance within the ploughing-dominant region yields Eq. (22). For a helix angle (ψ), the length of the helical cutting edge for an axial depth of cut of a_p is also considered. However, the minor variations in uncut chip thickness and forces experienced by different points on the cutting edge owing to its helical curvature is neglected as the lead of the helix (2,721 μm) is significantly larger than the axial depth of cut (50 μm). A factor $C_P = 0.7$ is also considered to neglect 30% of the forces that occur owing to elastic-regain [54]. Solution of this equation gives the expression for $n_{ploughing}$ for the ploughing region (Eq. 23).

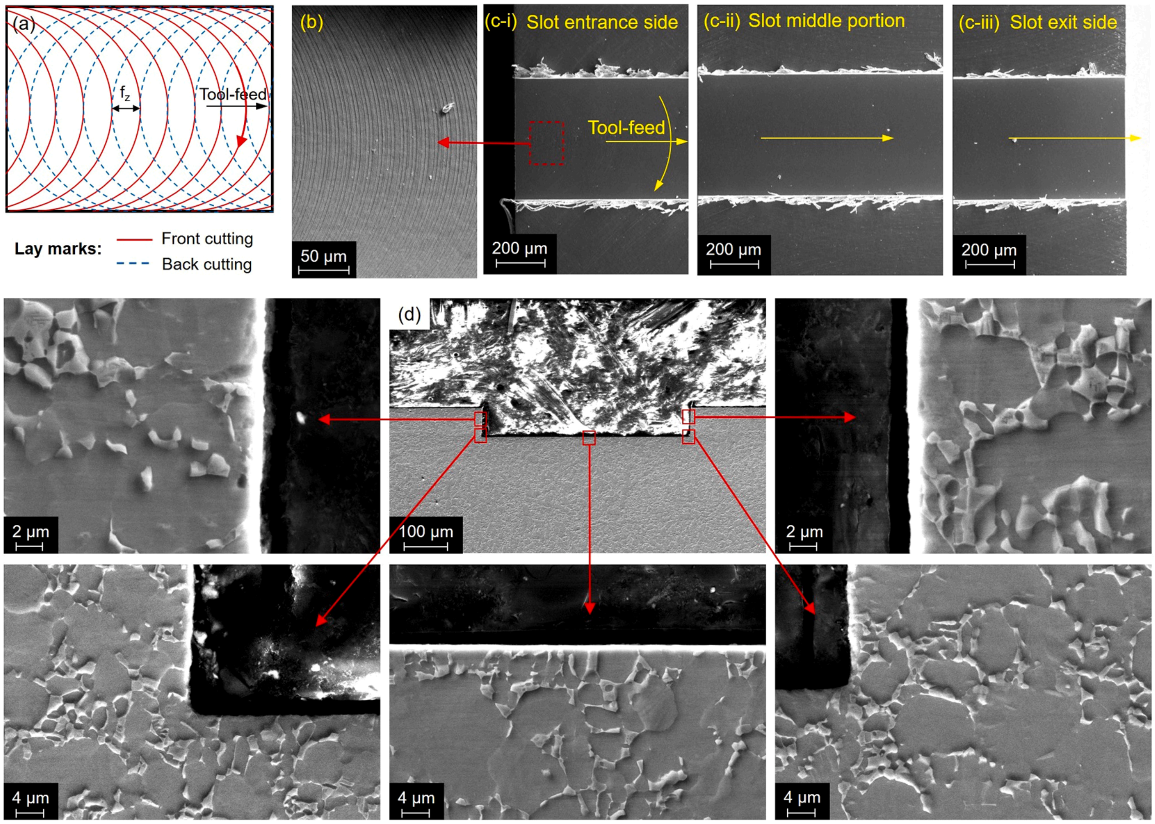

Fig. 9. Ensuring the uniformity among the generated chips: (a) schematic of the front-cutting and back-cutting lay marks that can generate on the micro-milled bottom surface, (b) magnified SEM image of the bottom surface of the micro-milled slot where only front-cutting lay marks can be observed, (c) SEM images of the slot in entrance-side, middle portion, and exit-side, (d) SEM images of the microstructures at different locations on the entrance-side cross-sectional view in dry micro-milling at 25,000 rpm speed, 4.0 µm/flute feed, and 50 µm axial depth

$$\left(\frac{2\tau_{ds}}{n_{ploughing}+1}\right)\left[\int_{0}^{h_{min}}\left\{1.285+\sin^{-1}\left(1-\frac{y_i}{r_e}\right)\right\}dy_i\right]\left(\frac{a_p}{\cos\psi}\right)=C_P F_{N,max}^{(Plough)} \tag{22}$$

$$\therefore n_{ploughing}=\frac{2\tau_{ds}a_p}{0.7\cos\psi F_{N,max}^{(Plough)}}\left[1.285h_{min}+\frac{\pi r_e}{2}-\sqrt{2h_{min}r_e-h_{min}^2}-(r_e-h_{min})\sin^{-1}\left(1-\frac{h_{min}}{r_e}\right)\right]-1 \tag{23}$$

On the other hand, force balance within the shearing-region over the entire chip-tool plastic contact length (up to K_B) yields the $n_{shearing}$ value. Beyond this K_B length, the chip also maintains elastic-contact for certain distance before completely separating from the tool surface. Maity and Das (2007) [55] highlighted that about 30–35% of the total cutting force contribute to elastic contact, while rest of the forces contribute to plastic contact. Assuming 70% of the normal force distributes over the chip-tool plastic-contact region, the force balance leads to the following equation from where index $n_{shearing}$ for shearing can be estimated.

$$\left(\frac{2\tau_{ds}}{n_{shearing}+1}\right)\left[\int_{h_{min}}^{r_e}\left\{1.285+sin^{-1}\left(1-\frac{y_i}{r_e}\right)\right\}dy_i+\int_{r_e}^{r_e(1+\sin\gamma_o)}\left\{1.285-sin^{-1}\left(\frac{y_i}{r_e}-1\right)\right\}dy_i+\int_{r_e(1+\sin\gamma_o)}^{K_B}(1.285-\gamma_O)dy_i\right]\left(\frac{a_p}{\cos\psi}\right)=0.7F_{N,\max}^{(shear)} \tag{24}$$

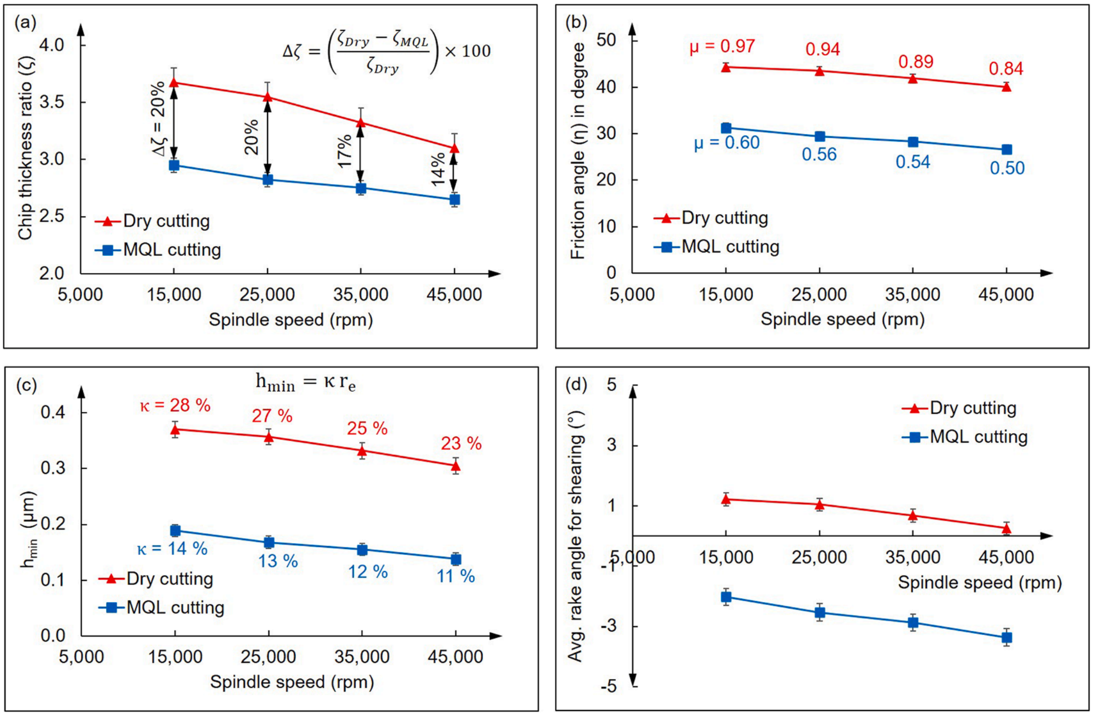

Fig. 10. Variations of the (a) chip thickness ratio with speed where Δζ shows the percentage capability of MQL in reducing the chip thickness ratio as compared to dry micro-milling, (b) friction angle with speed where the apparent coefficient of friction values are also indicated, (c) minimum uncut chip thickness h_{min} for ploughing-to-shearing transition for a given edge radius with speed, and (d) weighted average orthogonal rake angle for shearing-dominant region with speed for dry and MQL assisted cutting

$$\therefore n_{shearing} = \frac{2\tau_{ds} a_p}{0.7\cos\psi F^{(shear)}_{N,\max}} \left[1.285(K_B - h_{\min}) - \gamma_O(K_B - r_e - r_e\sin\gamma_o) + (r_e - h_{\min})sin^{-1}\left(1-\frac{h_{\min}}{r_e}\right) + \sqrt{2h_{\min}r_e - h_{\min}^2} - \gamma_O r_e - \sqrt{(r_e)^2 - (r_e\sin\gamma_o)^2}\right] - 1 \qquad (25)$$

4. Results and discussion

For the assessment of the failure criteria of the micro-milling tool, the first requirement is to obtain the chip thickness ratio (ζ). However, measurement of chip thickness for every trial is a cumbersome task; and thus, ζ is initially expressed as a function of uncut chip thickness using a small number of experiments. Thereafter, the other essential parameters such as apparent friction coefficient, minimum uncut chip thickness, shear-dominant rake angle, etc. are sequentially estimated. Since the edge-chipping does not occur within the first 5.0 mm length of cut, the variation of the tool features with the progression of micro-milling is demonstrated. Conditions for the onset of various wear modes for varying process parameters and lubrication condition are also assessed. Finally, the edge-chipping pattern and condition are validated considering the progressive changes in worn-out tool geometry and tribo-pair scenario.

4.1. Chip thickness and chip thickness ratio

For macro-scale machining, the chip thickness is conventionally measured by mounting the collected chips in a suitable medium and polishing the same before observing under a microscope. Such a procedure is not suitable for micro-milling chips as they can easily break and distort under slight mounting pressure owing to its very small thickness (10 – 15 μm). Therefore, for measuring the thickness, micro-milling chips are first collected by placing a both-sided carbon adhesive tape at the vicinity of cutting zone during the experiments. End-milling inherently produces discontinuous chips as at least one chip is generated by each cutting edge per revolution of the tool. Accordingly, around 1,250 chips are generated during cutting 5 mm slot with 4.0 μm/flute feed. A large number of such micro-chips gets automatically adhered to the carbon tape, which are then observed under an SEM (Fig. 8a). However, the chip thickness also varies along its length similar to the variation of uncut chip thickness. The chip thickness becomes maximum only at one point along its length, as discussed by Saha et al. (2020) [56]. From the magnified image of a favourable chip, the average thickness is measured in successive points along its length by suitably orienting the SEM sample holder. A convex-shaped curve (Fig. 8b) can be obtained when the measured chip thickness values are plotted. The maximum chip thickness can thereafter be obtained from the zenith of such curve. A similar strategy for measuring chip thickness in macro-scale milling was also reported by Benjamin et al. (2018) [57].

To understand the variation of ζ with h_i, a preliminary experimentation is carried out with varying f_z ranging from 1 – 4 μm/flute but constant speed of 25,000 rpm and depth of cut of 50 μm. For the fresh tool having 1.3 μm edge radius, the minimum uncut chip thickness (h_{min}) is expected to be around 0.39 μm (considering h_{min} as 30% of the edge radius) [44]. It is usually customary to select the feed per flute value higher than the corresponding h_{min}. Accordingly, a substantially higher feed range (1 – 4 μm/flute) was selected expecting shearing of the workpiece material by every cutting edge in each tool rotation. Now, for each feed value, the maximum chip thickness (a_2) is measured and

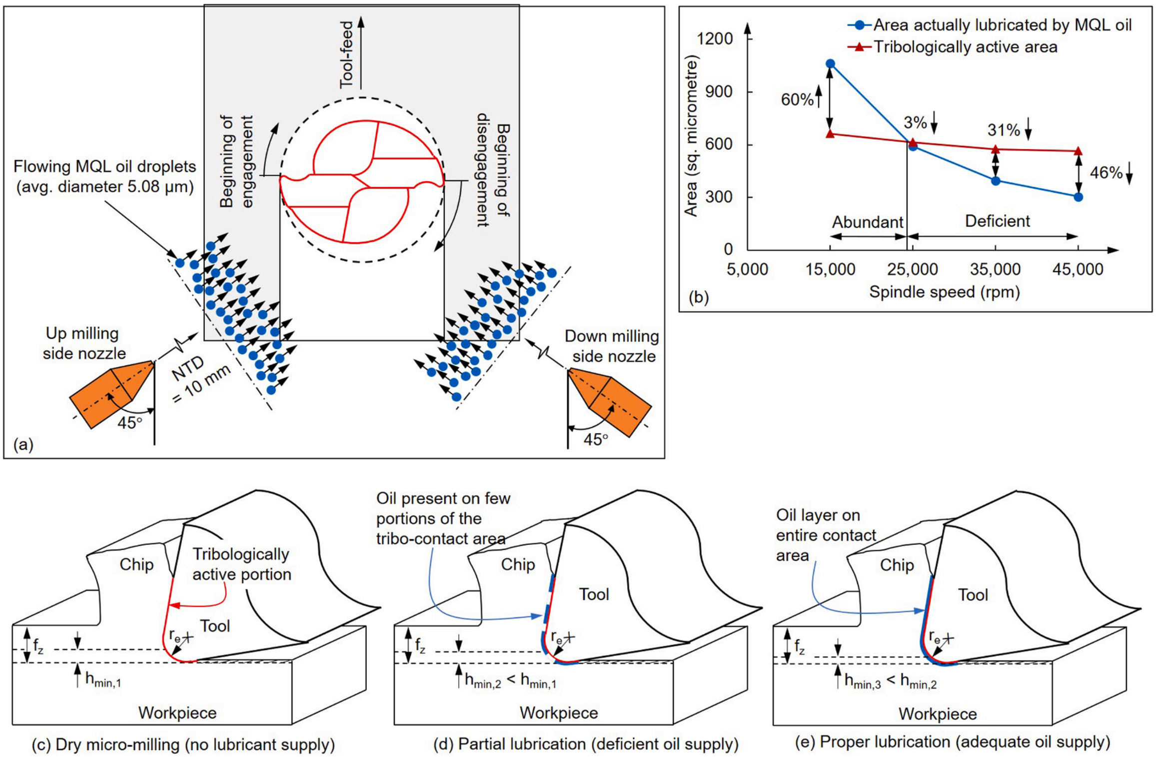

Fig. 11. (a) Schematic representation of the application of MQL oil droplets directly on the cutting edges during the disengagement period using two nozzles placed behind the tool along the tool-feed direction maintaining 10 mm nozzle-tool distance, (b) capability of the 6 ml/h MQL oil flow rate in wetting the entire tribologically active area during the disengagement half-cycle for varying speed, retrieved by extending an analysis of the authors Saha et al. (2020) [56], and (c-e) micro-milling in dry condition, deficient oil supply condition, and adequate oil supply condition, and the corresponding variation in minimum uncut chip thickness

corresponding ζ value is calculated. With reference to the investigation of Wojciechowski et al. (2019) [58], it is also worth mentioning that the chip thickness accumulation can play dominating role when the ratio (h_{min}/f_z) remains higher than 0.19. However, in the current work, the reported chip thickness ratio does not subsume the accumulated residue uncut material. As shown in Fig. 8c, a decreasing tendency of ζ with feed is observed. The average rake angle becomes less negative when a higher feed per flute is employed for a given tool. Thus, with an increase in f_z, the extent of shear deformation decreases leading to a relatively smaller chip thickness, and hence, smaller ζ. The variations of ζ for dry and MQL assisted cutting can be expressed using the following second degree polynomial equations.

$$\zeta_i^{Dry} = 0.315h_i^2 - 2.489h_i + 8.465 \tag{26a}$$

$$\zeta_i^{MQL} = 0.275h_i^2 - 2.437h_i + 8.230 \tag{26b}$$

In precision material removal processes with highly negative rake angle, the microstructure of the workpiece material and corresponding grain-level variation can also affect chip formation mechanism. Rahman et al. (2021) [59] showed that grain heterogeneity and crystallographic orientation can induce non-uniformity in lamella formation in the serrated micro-chips; however, such effect is mostly perceptible in nano-scale machining. Sun et al. (2021) [60] also showed that the cutting forces and chip formation mechanism were affected by the grain size and dislocation density in precision machining. To study the effects of microstructural factors, the cross-section at the tool-entrance side of the polished micro-milled slot for dry cutting is observed under the SEM (Fig. 9d). The enlarged view of the slot side walls, bottom corners, and slot centre are also shown. It can be observed that the cutting mostly proceeds through the grains. No evidence of grain pull-out and grain pass-over is detected. Kieren-Ehses et al. (2021) [61] highlighted that the effects of workpiece grain orientation, size, and distribution on micro-milling performance can be perceived at lower speeds, typically below 7,000 rpm (1.1 m/min). In the current investigation, cutting speed is selected adequately high (23.6 – 70.7 m/min), and thus significant effects of grain orientation on the micro-milling performance is not expected. Additionally, sub-surface deformed layer that is characterized by the elongated or compressed grains [30] cannot be observed here. Absence of such sub-surface deformed layer can be attributed to the significantly low cutting forces (in the order of 0.5 N) and low cutting zone temperature that are insufficient for deforming Ti-6Al-4V. Given the more-or-less homogeneous grain size of individual phases and uniform phase distribution of the workpiece material (Fig. 1g), the effect of material inhomogeneity on chip thickness can be neglected as the current investigation is primarily focused on the tool wear study.

Furthermore, a favourably oriented chip is randomly selected for thickness measurement, and thus, it is pertinent to ensure uniformity in thickness among the generated micro-chips. Tool run-out and tool-bending (chip accumulation) can also induce variation in chip thickness. Similar to every tool-based machining process, lay marks also inherently generate during micro-milling process owing to the simultaneous rotational and linear relative motions with respect to the workpiece. When every cutting edge in each tool rotation participates in material removal, uniform front-cutting lay marks are generated on the bottom surface, as schematically shown in Fig. 9a. The front-cutting lay marks are identified by the convex shape with respect to the tool-feed direction. In absence of tool bending, the linear distance between two adjacent lay marks when measured along the feed direction at the slot centre matches with the set feed per flute [62]. Presence of tool run-out, phase difference, or bending also leads to the generation of back-cutting lay marks that are identified by the concave shape with respect to the tool-feed direction [63,64]. As shown in Fig. 9b, homogeneous and uniformly distributed front-cutting lay marks are generated on the bottom surface. Additionally, five lay marks can be detected in a linear distance of 20 μm that matches with the set feed per flute (4 μm/flute). No sign of back cutting on the whole bottom surface can be detected.

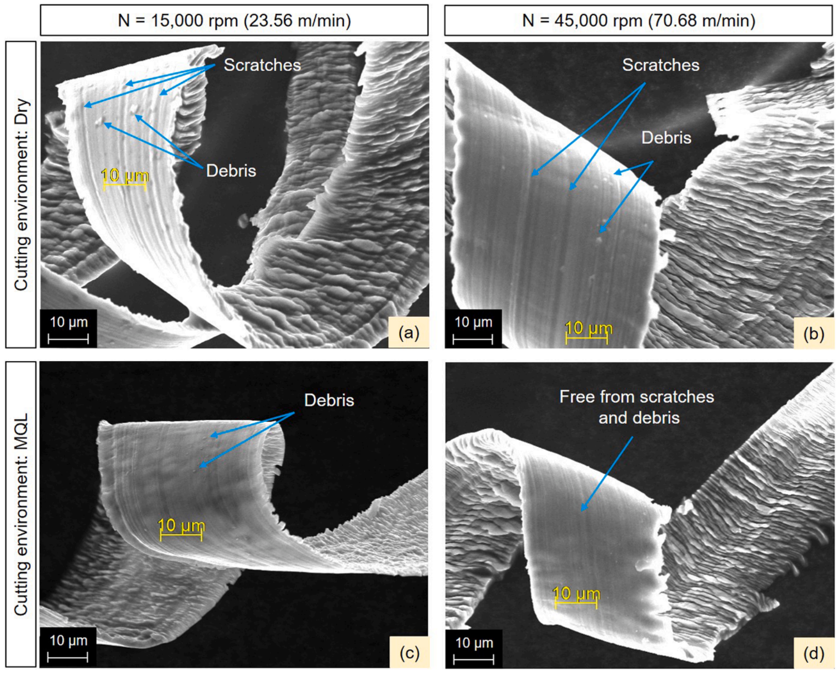

Fig. 12. Under-side of the chips showing the presence of scratches and dislodged adhered material for different cutting velocities in dry and MQL micro-milling of first slot. Significant presence of scratches and debris on the under-side, which are the indications of high friction at chip-tool interface, can be observed at low speed dry cutting. With the increase in speed and application of MQL fluid, presence of such frictional elements reduces considerably

Thus, the effects of tool run-out, phase difference, and bending can be assumed to have negligible influence on the chip thickness.

4.2. Influences of MQL during sustainable micro-milling

Proper lubrication assists in smooth flow of the chips that helps in reducing the degree of shear deformation. Thus, for same uncut chip thickness, a lower chip thickness ratio (ζ) is expected for MQL assisted cutting as compared to that of the dry cutting. The same can be observed from Figs. 8c and 10a. Regardless of the lubrication, the chip material becomes more plastic at higher cutting velocity, and thus, the frictional resistance at the chip-tool interface reduces [65]. The easiness in chip flow leads to the reduction of shear deformation and chip thickness. This explains the monotonically decreasing nature of ζ with cutting velocity (Fig. 8a). The difference in ζ value between dry and MQL cutting (Δζ in Eq. 27) also changes with the speed. A positive Δζ value indicates that MQL application can advantageously reduce the chip thickness as compared to dry cutting. The higher is the Δζ, the more efficient is MQL

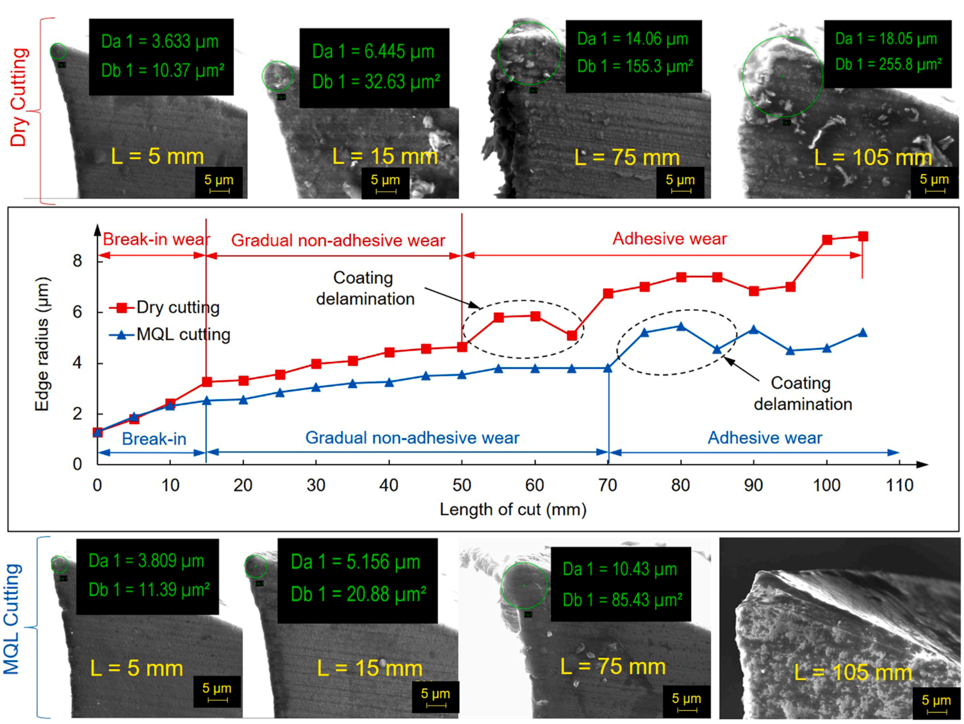

Fig. 13. Tool-life curve showing typical variation of the edge radius with length of cut for dry and MQL assisted micro-milling at 25,000 rpm speed, 4 μm/flute feed and 50 μm axial depth. Different stages of tool wear (rapid break-in wear, gradual abrasive and non-adhesive wear, coating delamination, and adhesive wear) are also shown within the graph. SEM images of the cutting edge after different lengths of cut is also given (edge-chipping occurred after 105 mm MQL cut, so edge radius cannot be measured accurately)

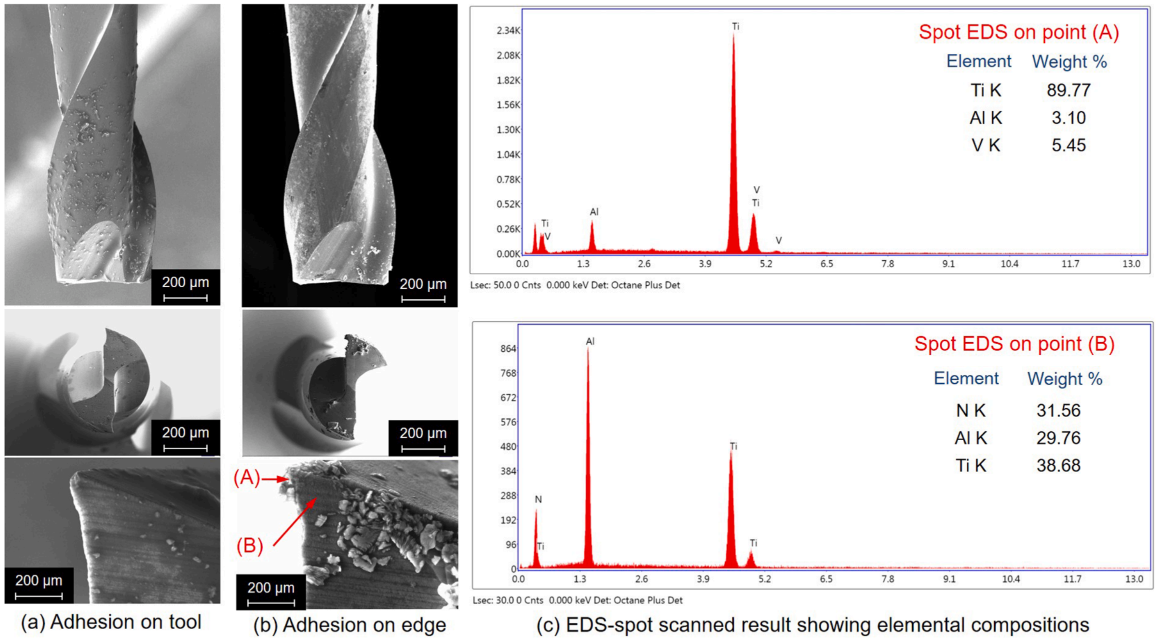

Fig. 14. (a) SEM images of the used tool showing loosely adhering deposits over the entire tool body that occurs right from the beginning of micro-milling; however, the cutting edge remains more-or-less unaffected, and (b) same tool after about 45 – 80 mm cut with adhesion at the cutting edge, and (c) EDAX spot analysis result to confirm adherence of Ti-6Al-4V workpiece material over the TiAlN coating of the tool

in reducing the chip thickness. As shown in Fig. 10a, the $\Delta\zeta$ is relatively high (20%) at low speed (15,000 rpm) and reduces to 14% at the highest speed (45,000 rpm).

$$\Delta\zeta = \left(\frac{\zeta^{Dry} - \zeta^{MQL}}{\zeta^{Dry}}\right) \times 100 \tag{27}$$

Primary goal of the MQL application in micro-milling is to lubricate the chip-tool-workpiece contact areas as the cutting temperature remains considerably low, typically 80 – 120°C [40]. However, for lubricating the contact surfaces, it is necessary to directly deposit the oil droplets on the cutting edges. In general, MQL oil droplets do not possess sufficient velocity (kinetic energy) to penetrate deep into the

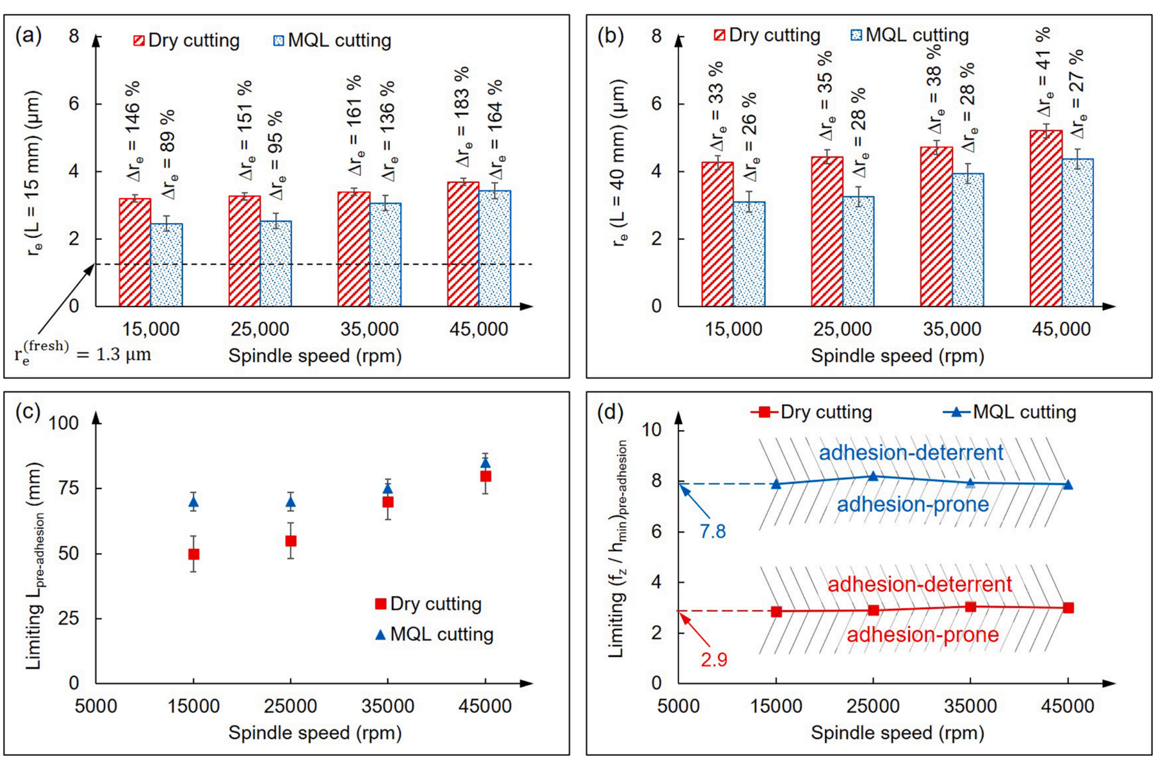

Fig. 15. Bar chart presenting the measured edge radius after (a) 15 mm, and (b) 40 mm length of cut for different spindle speeds in dry and MQL cutting, (c) variations of the limiting length of cut after which strongly adhered deposits on the cutting edge, and (d) variations of the ratio between feed and minimum uncut chip thickness at the limiting length of cut showing the adhesion-deterrent and adhesion-prone regions

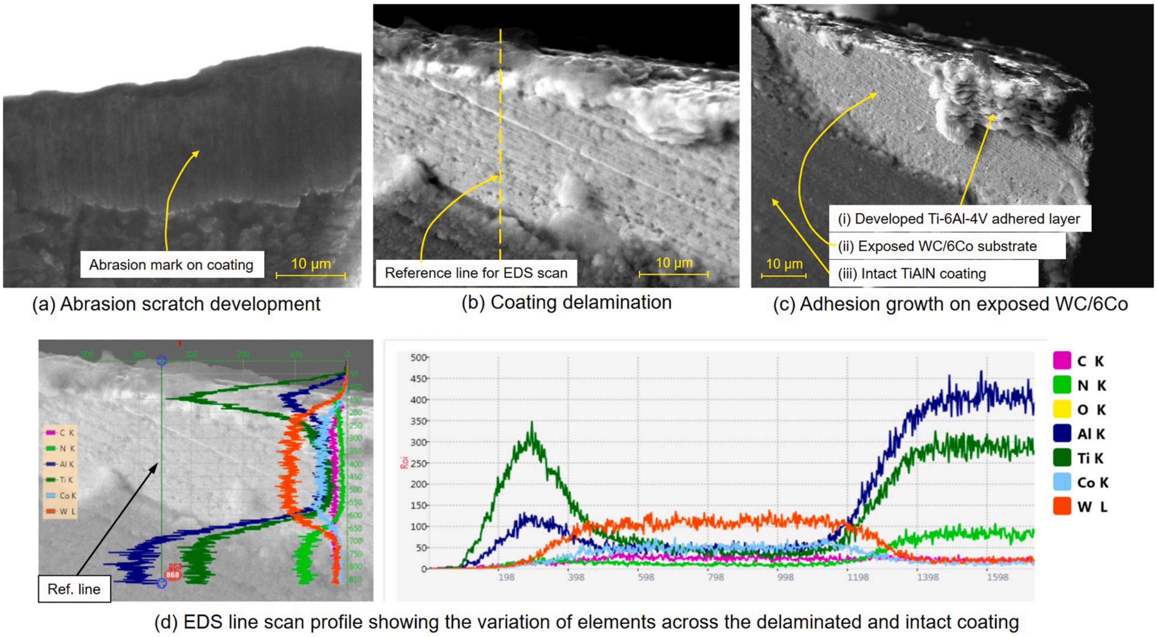

Fig. 16. Typical rake face of the used tool showing (a) the region that suffers abrasion at the beginning of micro-milling, (b) subsequent delaminated of coating with further micro-milling, (c) growth of adhered layer on the exposed WC/6Co substrate with the further machining, and (d) EDS line scan result to ensure peeling off of the TiAlN-coating from the tungsten carbide substrate

chip-tool-workpiece contact zone owing to high tribo-contact pressure. However, in this experimentation, two nozzles are placed behind the tool along the feed direction so that the oil droplets can be directly deposited on the cutting edges during their 180° disengagement period (Fig. 11a). Owing to very small droplet size (average diameter 5.08 μm), each oil droplet can lubricate a small area when deposits on the cutting edge. Thus, a finite number of droplets are required to deposit on the tribologically active portion of the rounded cutting edge during the disengagement period for achieving efficient lubrication. However, as the rotational speed of the tool (N) increases, the disengagement period (T_{dis}) also reduces following Eq. (1). So less time is available to deposit oil droplets on the cutting edges at higher speeds. Accordingly, entire chip-tool-workpiece contact region cannot be lubricated during the disengagement period at higher speeds. Consequently, machining is carried out under deficient lubrication condition when speed exceeds a certain limit.

In an earlier investigation [56] by the authors using the same set-up, it was established that 6 mL/h oil flow rate is abundant for 15,000 rpm, adequate for 25,000 rpm, and deficient for higher speeds. As shown in Fig. 11b, about 60% more area can be lubricated at 6 mL/h flow rate within the disengagement period available at 15,000 rpm. Under the same flow rate as speed increases to 25,000 rpm, lesser time is available to immerse tribologically active areas, and 3% less area can be lubricated within the corresponding disengagement period. The deficiency further increases with the increase in speed. The oil flow rate is kept unchanged in the current work too so that the influences of abundant, adequate and deficient MQL supply can also be investigated. When the oil supply becomes deficient, the MQL assisted cutting approaches towards the dry cutting. Accordingly, the effect of MQL cannot be perceived properly under deficient lubrication condition. Thus, the $\Delta\zeta$ value in Eq. (27) is higher (or MQL is more effective in reducing the chip thickness) at lower speeds owing to the abundant or adequate oil supply. With an increase in speed beyond 25,000 rpm, MQL becomes less efficient owing to the deficient supply of oil, and thus, $\Delta\zeta$ reduces gradually.

For unchanged tool geometry and feed per flute, the weighted average orthogonal rake angle (Eq. 12) is constant to $\gamma_{avg} = -19.1°$. However, as ζ varies, the shear angle and friction angle vary. A lower ζ value indicates less frictional resistance at the chip-tool interface, and thus, the pattern of variation for both ζ and η with speed is expected to be similar (Fig. 10a-b). The "apparent coefficient of friction" at the tribo-contact region is found to be very high (0.84 – 0.97), especially in dry cutting. Through pin-on-disc tribological experiment, Liang et al. (2020) [66] also observed a high coefficient of friction in the order of 0.88 between Ti-6Al-4V and WC/6Co pair at low temperature for short running period. The apparent friction coefficient reduces when cutting velocity is increased as well as when MQL is applied. Reduction in apparent friction coefficient with the increase in speed was also reported by Miguélez et al. (2013) [67]. The under-side (shining surface) of the chips also reflects such changes in apparent friction coefficient. As shown in Fig. 12, under-side of the chip in dry cutting at lowest velocity (23.56 m/min) is characterized by the significant presence of scratches and dislodged debris of the adhered material. These are the characteristics of high friction coefficient where the chip material tends to adhere to the rake surface and the smooth flow of the chips is restricted. Such scratches and debris reduce significantly as speed increases to 70.68 m/min in dry cutting. Chips for high-speed MQL cutting are mostly free from scratches and debris, which is the indication of lower friction at the chip-tool interface.

Reduced coefficient of friction (μ) also has a favourable impact on the minimum uncut chip thickness (Fig. 10c). For a given fresh edge radius of 1.3 μm, the h_{min} in dry cutting remains in between 0.30 – 0.37 μm (i.e. 23 – 28% of r_e). The same reduces to 11 – 14% of r_e in MQL micro-milling. Whereas the γ_{avg} value is constant, the rake angle for shear-dominant region $\gamma_{avg}^{(shear)}$ depends on the h_{min} value (Eq. 14). As usual, $\gamma_{avg}^{(shear)}$ is less negative than γ_{avg} owing to the exclusion of tool-tip within h_{min} thickness. The effect of rounded-tip at the cutting edge on chip shearing reduces as h_{min} increases. Since MQL assisted cutting offers lower h_{min}, the corresponding $\gamma_{avg}^{(shear)}$ is more negative as compared to that obtained in dry cutting (Fig. 10d).

4.3. *Progression of micro end milling tool wear through different stages*

When a fresh tool is engaged in micro-milling, initially it undergoes rapid wear that is predominantly abrasive in nature. This initial rapid wear is termed as "break-in" wear that continues up to 10 – 15 mm

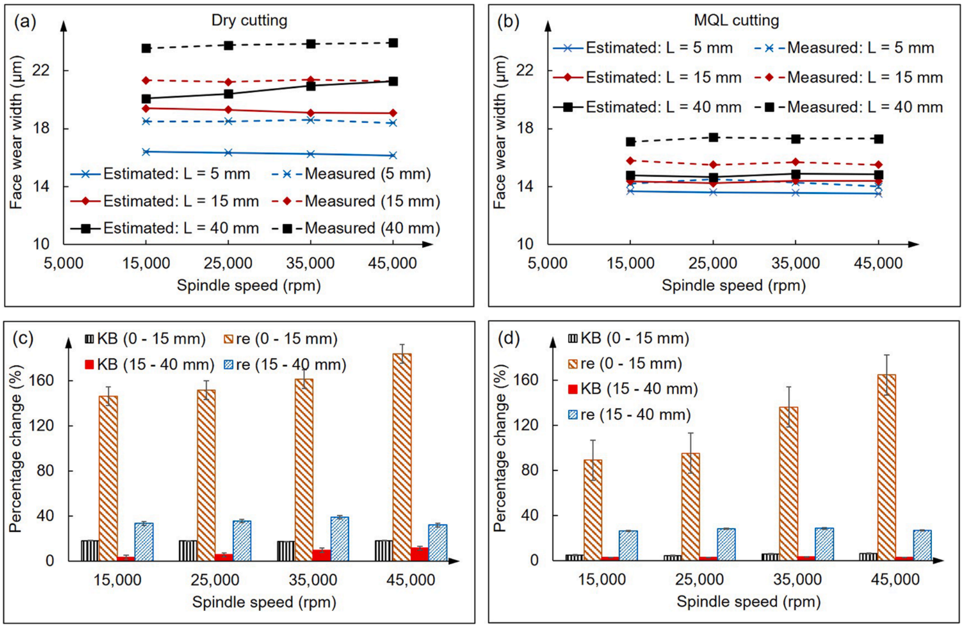

Fig. 17. Estimated and measured values of the width of the wear track on the rake surface after different lengths of cut for (a) dry and (b) MQL based micro-milling; percentage increase of the edge radius and wear track width within 0 – 15 mm and 15 – 40 mm segments of the length of cut for (c) dry and (d) MQL based micro-milling

length of cut. During this period, the edge radius increases steeply but the cutting edge retains its shape. Signs of other wear (like coating delamination, chipping, etc.) are not observed during this break-in wear zone. A typical tool wear progression curve is shown in Fig. 13.

A steady and gradual rate of increase in edge radius can be noticed after the break-in wear zone. Initial phase of this steady-state wear proceeds predominantly through mechanical abrasion. Occasional adherence of the chip is also observed in this zone; however, such adhesive deposits are loose and distributed sparsely over the entire tool (Fig. 14). Such deposits are less likely to influence material removal mechanism since these are located far away from the active portion of the cutting edges. These loosely adhering deposits can also be easily blown away using air flow. Gradual increase in edge radius through abrasion is accompanied by the reduction in coating thickness at the cutting edge. Accordingly, after a certain length of cut, coating gets removed completely. The tribo-contact pair changes from “workpiece-coating” to “workpiece-substrate” after this coating delamination (peeling off). Such change in the tribo-pair induces edge chipping, as discussed in the successive sections.

Soon after the delamination, the cutting edge undergoes severe adhesive-abrasive wear. Unlike pre-delamination loose adhesions over the entire tool, this post-delamination adhesions are thick and strongly welded with the cutting edge. Edge radius also increases steeply based on the size of the adhered deposit at the edge. Formation, growth, and disappearance of adhered material occur sequentially and repetitively when such delaminated tools are continuously used for machining. This adhered material initially protects the tool from further abrasion or chipping. However, as soon as the adhered layer gets dislodged, edge chipping takes place, as discussed in details through stress analysis in section-4.5. Edge chipping leads to significant change in tool-edge geometry. Often multiple edges produce leading to the difficulty in measuring edge radius. Thus the edge radius cannot be used for quantifying tool wear post-chipping, rather flank wear length and crater wear length are better indices in characterizing the wear scenario. Since the earlier presented model is developed based on a rounded-edge, further analysis is kept confined to pre-chipping region.

The degree of increment of the edge radius within the 15 mm characteristic length of break-in wear is shown in Fig. 15a. Edge radius steeply increases to 3.20 – 3.69 µm within initial 15 mm dry cut. This is equivalent to 146 – 183% increase within the break-in wear zone. Application of MQL, however, shows a relatively lower increase in edge radius within this rapid wear zone. After 15 mm MQL cut, edge radius increases to 2.46 – 3.44 µm that is equivalent to 89 – 146% increase compared to fresh tool. As usual, abrasion wear rate is more at higher speed owing to higher relative velocity between chip-tool. In this matter, the lower is the Δr_e (Eq. 28), the more efficient is the MQL lubrication in reducing tool wear rate. At 15,000 rpm, Δr_e for MQL cutting is substantially lower than that of dry cutting. As speed increases, this gap in Δr_e between dry and MQL reduces. The lower efficiency of MQL at higher speeds can be attributed to the deficient lubrication condition that occurs when speed exceeds 25,000 rpm, as discussed earlier in section-4.2.

$$(\Delta r_e)_{0-15} = \left(\frac{r_{e,15mm} - r_{e,fresh}}{r_{e,fresh}}\right) \tag{28}$$

$$(\Delta r_e)_{15-40} = \left(\frac{r_{e,40mm} - r_{e,15mm}}{r_{e,15mm}}\right) \tag{29}$$

After the rapid wear zone, tool experiences a gradual wear that is non-adhesive in nature, for certain length of cut. The limiting length of cut before the sign of strong adhesion also varies with the speed and cutting environments (Fig. 15c). MQL assisted cutting offers longer cutting length prior to the occurrence of adhesion. High relative velocity between chip-tool also hinders the adhesive layer formation, and thus, higher speeds offer longer adhesion-free cutting length. A characteristics length of 40 mm is considered for comparison purpose as adhesion started appearing after 45 mm in dry cutting at the lowest speed under investigation. The rate of increase in edge radius (Δr_e in Eq. 29) in the gradual non-adhesive wear zone is significantly less as compared that in break-in wear zone (Fig. 15b). With 33 – 41% increase over a cutting length of 25 mm, the edge radius becomes to 4.27 – 5.21 µm after total 40 mm length of dry cut. Similarly, edge radius increases to 3.11 – 4.37 µm after 40 mm MQL cut.

As the edge radius increases with the progression of milling, the minimum uncut chip thickness also increases proportionally following the relationship ($h_{min,i} = \kappa r_{e,i}$). However, the feed per flute remains

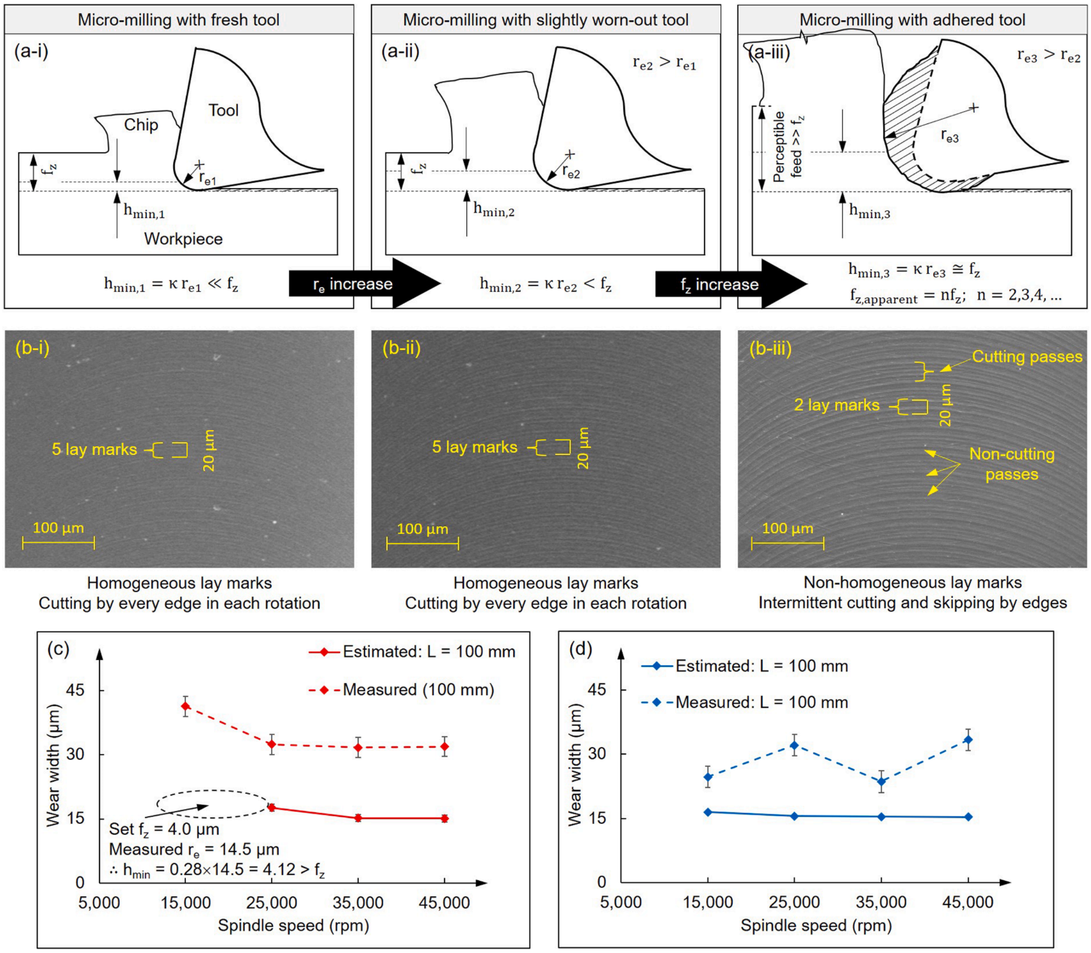

Fig. 18. Schematic representation of the material removal scenario (i) for a fresh tool with $f_z \gg h_{min}$, (ii) for slightly worn-out tool with $f_z > h_{min}$, (iii) for an adhered tool with apparent f_z few times higher than set f_z owing to intermittent non-cutting passes; (b) SEM images of the bottom-surface of the micro-milling slot under corresponding conditions; and (c-d) variations of the estimated and measured K_B after 100 mm cut in dry and MQL micro-milling

unchanged to f_z = 4 µm/flute. Interestingly, the ratio $\left(\frac{f_z}{\kappa\, r_{ei}}\right)$ at the limiting scenario just before adhesion occurrence remains more-or-less constant over the range of speed investigated here (Fig. 15d). For dry cutting, this limiting (f_z/h_{min}) = 2.90. For MQL assisted cutting, the corresponding ratio is about 7.80. Therefore, it can be inferred that, with the gradual increase in h_{min} with the progression of micro-milling, tendency of the strong adhesion formation at the cutting edge becomes high as soon as the h_{min} exceeds 12% (for MQL) or 34% (for dry) of the set feed per flute. It also emphasized the necessity of selected relatively higher feed per flute during micro-milling experiments to ensure adhesion-free micro-milling.

It is also worth mentioning that the h_{min} in MQL assisted cutting remains significantly less owing to low κ values. Accordingly, a feed per flute value higher than 7.80 times h_{min} may not be significant enough to induce tool breakage. For an example, for 1.2 µm edge radius and 15% κ, the minimum feed per flute with MQL cutting should be 1.4 µm in order to avoid quick adhesion of chip material. A significantly higher (2 – 3 times) value than this limiting one may be preferred to allow provision for gradual wear with the length of cut. It also highlights the reason behind quick adhesion observed by different researchers [36] within very small length of cut during micro-milling using a relatively smaller feed per flute. With the gradual increase in edge radius, the onset of occurrence of strong adhesion at the cutting edge can be mathematically expressed as follows.

$$r_{e,i} \geq \begin{cases} \dfrac{f_z}{7.8\,\kappa_{MQL}}, & \text{for MQL cutting} \\ \dfrac{f_z}{2.9\,\kappa_{Dry}}, & \text{for dry cutting} \end{cases} \tag{30}$$

4.4. Face wear width and its variation with progressive tool wear

Estimation of the face wear width (K_B) can be carried out following the procedure discussed earlier in section-3.3 through the measurement of abrasion mark (Fig. 16). Estimated and measured values K_B after 5 mm, 15 mm, and 40 mm length of cut are shown in Fig. 17a-b. Although the κ values are lower at higher speeds, a reduction of merely 17% in κ value is observed for 300% increase in speed (Fig. 10c). Accordingly, K_B also reduces with speed in most of the cases; however, only marginally. For example, only 1.57% lower K_B is recorded for L = 5 mm when speed is increased three-fold from 15,000 – 45,000 rpm. For a given set of f_z and κ values, K_B values also increase progressively with the length of cut as the edge radius increases. MQL assisted cutting exhibits lower κ values as well as lesser edge radius after same length of cut. The cumulative effect of low κ and r_e in MQL assisted cutting results in significantly lower K_B values as compared to the corresponding cases of dry cutting.

The higher measured values of the face wear width (K_B) as compared to the estimated ones can be attributed to the following two aspects.

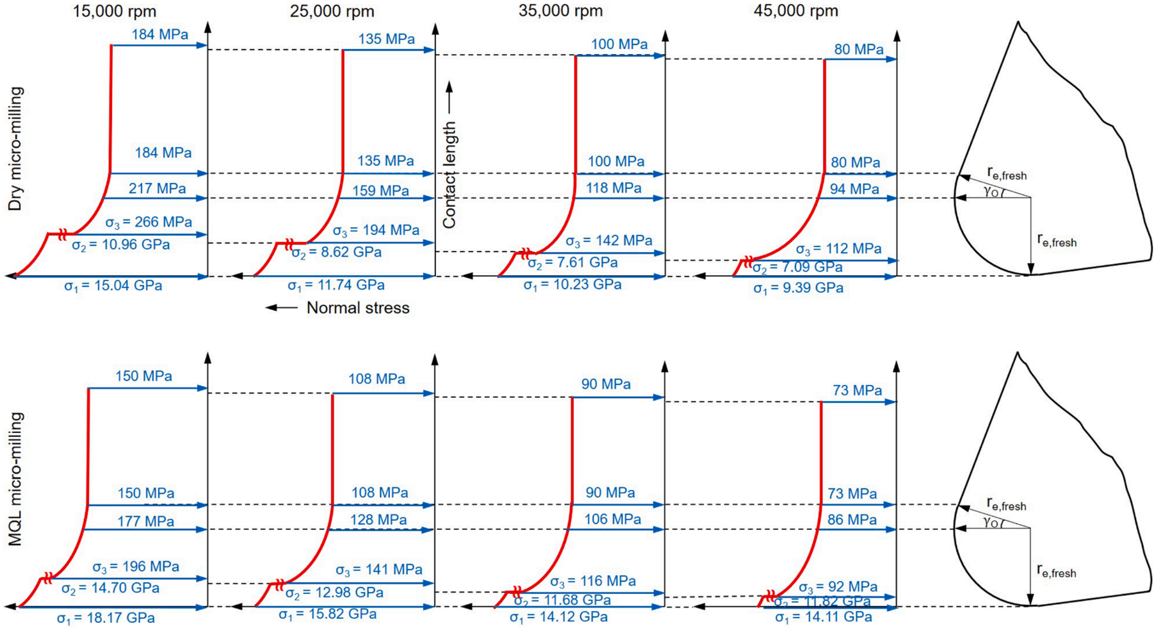

Fig. 19. Schematic of the normal stress profile for the fresh micro-milling tool under different speeds and cutting environments: σ_1 and σ_2 stress components having very high intensity are within ploughing-dominant region, while other components are within shearing-dominant region. With the increase in speed, both the stress intensity and minimum uncut chip thickness decrease. MQL cutting is associated with high ploughing stress, and thus, application of MQL can induce early edge-chipping if the coating or substrate material fails to tolerate it

- In theoretical estimation, face wear width (K_B) is calculated solely from the plastic-contact length between the chip-tool interface. In actual machining scenario, the chip also maintains a small length of elastic-contact slightly beyond the plastic-contact, as schematically shown in Fig. 7c. Although elastic-contact is less likely to abrade material from the tool surface, repeated rubbing can abrade material for a smaller length particularly towards the plastic-to-elastic transition line. The higher measured values of K_B as compared to the estimated ones can be attributed to the abovementioned contribution of elastic-contact on the abrasion of tool material. With MQL, presence of lubricant layer on the elastic-contact zone prevents the chip to come in physical contact with rake surface, and thus, the difference between measured and estimated values of K_B is less for MQL cutting.
- In addition, the chip is assumed to flow in the orthogonal direction during the theoretical analysis. However, owing to the presence of helix angle, chip flow direction deviates from the orthogonal plane. Accordingly, the contact length and face wear width (K_B) change slightly from the estimated one.

The percentage changes in K_B and r_e within the break-in wear (0 – 15 mm) and gradual non-adhesive wear (15 – 40 mm) zones is shown in Fig. 17c-d. Edge radius changes rapidly in the break-in wear zone, and thus, a considerable increase in K_B is also noticed. Within the gradual non-adhesive wear zone, K_B increases marginally owing to the low rate of increase in edge radius in this zone. Within initial 15 mm length of dry cut, when edge radius increased by 146 – 183%, the corresponding K_B increased by only 17 – 19%. In between 15 – 40 mm length of dry cut, when r_e increased by 31 – 38%, K_B increases only 4 – 11%. Similarly, for MQL assisted cutting within first 15 mm length of cut, 4 – 6% increase in K_B is noted when r_e increased by 90 – 164%. In between 15 – 40 mm MQL cut, K_B increased by only 2 – 3% while r_e increased by 26 – 26%. In the pre-adhesion regime, edge radius has the maximum effect on K_B while κ has a marginal effect. Although feed per flute remains unchanged in the pre-adhesion regime, it changes automatically after the onset of adhesion as discussed below.

Strong adherence of material at the cutting edge increases the edge radius in an unpredictable nature. When the edge radius becomes abnormally high, the corresponding theoretical h_{min} reaches close to the set f_z value. Sometimes theoretical h_{min} can even exceed the set feed. For such high values of h_{min}, each cutting edge fails to remove workpiece material in every tool rotation. Instead, the tool bends opposite to the feed direction to allow accumulation of uncut material ahead of it. Such free-rotation of the tool continues for few rotations, and thereafter the entire accumulated uncut chip is removed in a single stroke. In such a scenario, the maximum uncut chip thickness becomes few times higher than the set feed. This scenario is schematically shown in Fig. 18a(i-iii). For a fresh tool, the h_{min} remains significantly lower than the set feed. As edge radius increases, the difference between f_z and h_{min} reduces. When thick adhesion occurs, the edge radius becomes abnormally high and h_{min} reaches close to f_z. Subsequently, tool rotates freely allowing accumulation of uncut chip ahead of it. Then entire accumulated uncut chip is removed in a single cutting-pass that results in a very high value of apparent uncut chip thickness. Such free-passes and cutting-passes repeat so long as thick adhesive layer exists on the cutting edge. The perceptible feed per flute in such cutting-passes remains few times (typically 2 – 4) higher than the set feed per flute.

Table 4
Mechanical properties of the workpiece, substrate, and coating

Property	Ti-6Al-4V	WC/6Co	TiAlN
Microhardness (GPa)	3.14	11.02	35.0
Young's Modulus (GPa)	115	200	380
Fracture toughness ($MPa\sqrt{m}$)	50.0	7.7	2.7
Compressive failure strength (GPa)	0.95	7.35	23.0

Presence of free-pass and cutting-pass can be easily detected by observing the lay marks at the bottom-surface of the micro-milled slot. Owing to synchronous linear motion of the workpiece and rotational motion of the tool, lay marks (feed marks) inherently produce on the micro-milled surfaces. The linear distance between two similar points on adjacent lay marks, when measured at the slot centre along the feed vector, matches with the set feed per flute. As shown in Fig. 18b-i, the lay marks on the bottom surface are homogeneously distributed when a

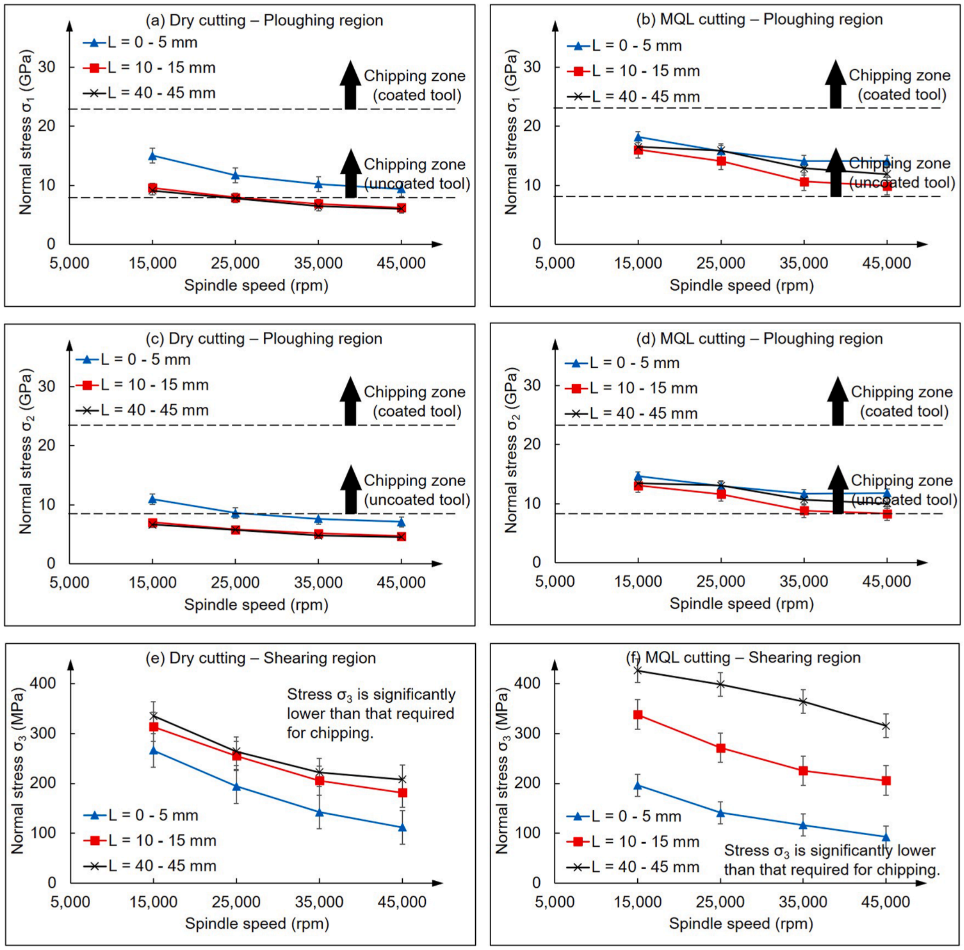

Fig. 20. Normal stresses in ploughing-dominant region (σ_1 and σ_2) and shearing-dominant region (σ_3) for dry and MQL cutting with varying lengths of cut under different speeds: the stresses are usually not high enough to induce edge-chipping for the TiAlN-coated tool; however, chipping can occur after delamination as σ_1 and σ_2 stresses mostly remain higher than the tolerable limit for WC/6Co substrate. Stress σ_3 is significantly low, and thus, it is not capable to induce chipping

fresh tool is used for micro-milling. At any arbitrary location, 5 uniform lay marks can be observed within a sample length of 20 μm that matches with the set feed (4 μm/flute). Surface generated during 40 – 45 mm length of cut also shows uniform lay marks. However, the surface generated after 100 mm length of cut is characterized by non-uniform lay marks that indicates existence of free-passes and subsequent cutting-passes. Within the free-passes, the distance between two lay marks is significantly larger than the set feed per flute. This indicates that each cutting edge in every tool rotation does not participate in chip shearing when strong adhesion occurs.

When chip-adhesion occurs, estimation of K_B becomes problematic owing to the unpredictable number of free-passes between two consecutive cutting passes. In addition, measurement of edge radius for an adhered tool is also associated with high percentage of error owing to the irregular shapes of the adhered material. Unpredictable nature of the formation, growth and disappearance of such adhered material are added difficulties in K_B prediction in post-adhesion period. As a result, significant difference between the measured and estimated values of K_B is noticed for both dry and MQL micro-milling after 100 mm cutting length (Fig. 18c-d).

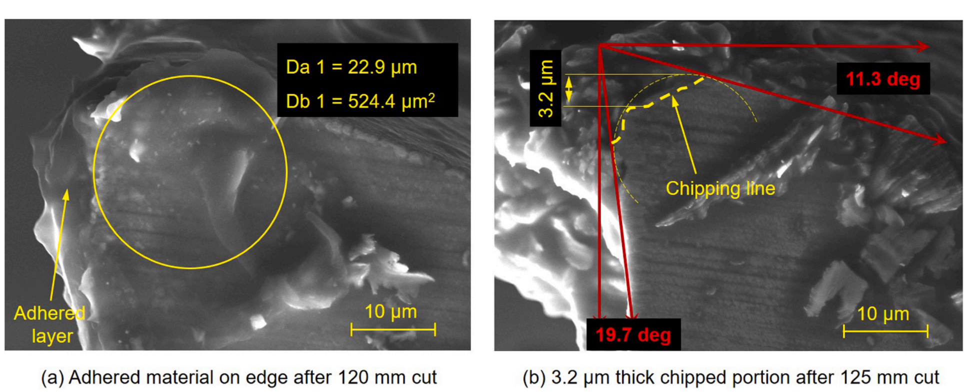

(a) Adhered material on edge after 120 mm cut (b) 3.2 μm thick chipped portion after 125 mm cut

Fig. 21. Occurrence of the edge chipping within 120 – 125 mm dry cut where the thickness of the chipped portion matches with the instantaneous h_{min} corresponding to the earlier pass

4.5. Normal stress variation and form-stability analysis

While gradual increase in edge radius is the primary mode of wear observed in the pre-adhesion period, edge chipping and catastrophic breakage of the tool-tip randomly occur during post-adhesion period. To assess the form-stability of the tool with the progression of micro-milling, variation of the normal stress acting on a fresh cutting tool is schematically shown in Fig. 19. As usual, the normal stresses acting within the ploughing region are significantly higher as compared to the corresponding stress in shearing region. The maximum normal stress, although finite, occurs at the extreme point of the tool-tip where instantaneous rake angle is -90°. With an increase in radial distance (y_i), the stress also gradually reduces as instantaneous rake angle becomes less negative. A steep drop in normal stress is also observed at the h_{min} line. Such drop in stress practically occurs over a narrow region within "Separation Deformation Zone" (Fig. 7a). As h_{min} and K_B lengths vary with the parametric conditions, the magnitude of normal stress also changes slightly even though the edge radius of the fresh tool is unchanged.

Relevant properties of the workpiece (Ti-6Al-4V), tool substrate (WC/6Co) [68], and tool coating (TiAlN) [69] are presented in Table 4. An indicative value of the ultimate compressive strength of the hard and brittle materials (substrate and coating) for micro-scale analysis is estimated following the suggestion of Fischer-Cripps [70]. Relatively low abrasion wear rate of the tool despite the presence of high normal stresses can be attributed to the large gap in micro-hardness between the workpiece and coating. Upon delamination, Ti-6Al-4V comes in direct contact with the WC/6Co. Although tool substrate material is harder than workpiece material, the hardness difference for WC-Ti64 pair is lower than TiAlN-Ti64 pair. This explains the relatively high tool wear rate observed in post-delamination period (Fig. 13). Considering both substrate and coating as brittle materials, chipping or fracture of the edge is most likely to occur whenever the external normal stress (σ_i) exceeds the ultimate compressive strength (σ_u) of the substrate or coating. Considering the presence of tensile residual stress (σ_{TRS}) within the coating, the chipping condition can be expressed as follows.

$$\sigma_i - \sigma_{TRS} \geq \sigma_u \tag{31}$$

As the stress components σ_1 and σ_2 are very high as compared to the other components, so the tip of the tool of thickness h_{min} is most vulnerable. However, in this investigation, all of the normal stress components including σ_1 and σ_2 for the fresh tool remain lower than $\sigma_{u,coating}$. Thus the tool remains intact and undergoes only abrasion at the initial stages. With the progression of micro-milling, the stress components within the ploughing-dominant region (σ_1 and σ_2) further reduces (Fig. 20). On the contrary, maximum stress within the shearing-dominant region (σ_3) increases with the length of cut. For a given feed per flute, higher r_e (or h_{min}) indicates lower thickness of the shear-able material that is associated with high degree of shear deformation and larger specific cutting energy. Accordingly, higher stress in shearing-dominant region is recorded for a worn-out tool. Furthermore, a fresh tool is more susceptible to edge chipping as σ_1 and σ_2 remain maximum for a fresh tool. It can also be inferred that, if a micro end milling tool can sustain first few millimetres length of cut without edge-chipping, it is less likely to catastrophically fail until coating-delamination. Although MQL has several benefits, it is associated with higher normal stresses as compared to the dry cutting. Thus a fresh tool engaged in MQL cutting has higher chance of suffering quick edge-chipping. This also explains the possible reason behind the unusual observation made by Ziberov et al. (2020) [18] where MQL micro-milling showed early edge chipping as compared to dry cutting.

With the gradual abrasive wear at the edge, adherent deposit starts forming as soon as the favourable condition (Eq. 30) is reached. Once the condition of Eq. (30) is reached, small size particles repeatedly adhere and disappear. When adhered material is dislodged, it mostly removes a thin layer of tool material with it. This leads to complete delamination of coating within just 15 – 20 mm length of cut in post-adhesion period. Thereafter thick and strong adhesion quickly forms over the entire tip of the tool owing to the high mutual affinity between Ti-6Al-4V and WC/6Co [71]. Growth and partial disappearance of thick adhered layer occur automatically during the micro-milling process. So long as the thick adhered layer exists over the tool, the edge is protected from breakage or chipping. As soon as the adhered layer dislodges completely or partially from the tool tip, the exposed WC/6Co substrate experiences high normal stresses. The stress components within the ploughing region (σ_1 and σ_2) mostly remain higher than the ultimate yield strength ($\sigma_{u,substrate}$) of the WC/6Co substrate. This results in brittle fracture of the tool-tip in the form of edge-chipping. Accordingly, width of the chipped portion mostly remain confine within the h_{min} value corresponding to the instantaneous edge radius just before chipping. After 120 mm cut (Fig. 21a), the instantaneous h_{min} for an edge radius of 11.4 μm remains around 3.1 μm. The same edge suffers chipping within next 5 mm length of cut (Fig. 21b). After 125 mm cut, the thickness of the chipped portion remains around 3.2 μm, which closely matches with the h_{min} corresponding to the earlier pass.

In this article, the tools are studied up to the first chipping. Until first chipping, the flank wear cannot be detected clearly under the SEM. Thus the flank wear length (V_B) can be considered an important parameter for quantifying micro-milling tool wear only after the chipping took place. It is also worth noting that the tools can be used even after chipping; however, at the cost of degraded surface integrity, dimensional tolerance, dynamic stability, and overall machinability. Repeated edge chipping after certain intervals continues until the tool catastrophically break. This final breakage does not usually take place before 500 mm length of cut. However, the tool may be considered to have exhausted useful service life much before the complete breakage. Progression of tool wear after first chipping until final breakage will be reported in a separate communication.

Conclusions

A comprehensive wear analysis for 500 μm diameter TiAlN coated WC/6Co tools during dry and minimum quantity lubrication (MQL) assisted sustainable micro-milling of Ti-6Al-4V is presented. Chip-tool-workpiece tribo-contact scenario is first assessed considering the process mechanics, lubrication, and the geometry of the rounded edge. Variation of normal stresses on the cutting edge is also evaluated from measured forces considering the gradually increasing nature of edge radius with the progression of micro-milling. Its consequences on the process mechanics are also studied in details. Based on the results, the following conclusions can be drawn.

Minimum uncut chip thickness (h_{min}) for ploughing to shearing transition can be reduced considerably through the application of MQL. The h_{min} value in dry micro-milling remains within 23 – 28% of the edge radius, with lower value obtained at higher speed. In MQL assisted cutting, the corresponding h_{min} reduces to 11 – 13% of the edge radius. The apparent coefficient of friction at chip-tool interface remains in the range of 0.84 – 0.97 in dry cutting, and reduces to a range of 0.50 – 0.60 with MQL.

When a fresh micro-tool is engaged for milling difficult-to-machine material, the tool wear successively proceeds through rapid abrasion, gradual abrasion, coating delamination, thick adhesion, and edge-chipping. Initially the fresh micro-mill experiences rapid abrasive wear up to 15 mm length of cut. During this rapid wear, edge radius increases from 1.3 μm to 3.69 μm (in dry cutting) and 3.44 μm (in MQL cutting). Thereafter, tool experiences a gradual non-adhesive wear up to 45 – 80 mm length of cut, which is followed by coating delamination and exposure of WC/6Co substrate. Application of MQL oil together with higher cutting speed helps extending this gradual non-adhesive wear regime.

As the edge radius increases with the progression of micro-milling, the corresponding h_{min} value also increases proportionally. In dry micro-milling, strong adhesion of chip material on the cutting edge begins to form once the instantaneous h_{min} of a worn-out tool exceeds 35% of the set feed per flute. In MQL cutting, such adherence occurs when corresponding h_{min} reaches 13% of the set feed. If otherwise permitted, usage of higher feed per flute (about 2 – 3 times of the fresh edge radius) is recommended to continue adhesion-free machining for a longer duration. Average face wear width (K_B) remains around 18.6 μm during dry micro-milling using a fresh tool of 1.3 μm edge radius at 4 μm/flute feed. Corresponding K_B can be reduced to about 14.2 μm using MQL.

Tip of the micro-end milling tool within the ploughing-dominant region experiences intense normal stresses in the range of 10 – 18 GPa. Thus, the tool-tip of thickness h_{min} is susceptible to fail through edge-chipping. Beyond h_{min} in the shearing-dominant region, stresses are not significant enough to induce chipping. As the tool experiences gradual wear, intensity of stresses within the ploughing-dominant region reduces. Thus, a fresh tool is more vulnerable to edge-chipping rather than an abrasively worn-out tool.

Despite offering several advantages, application of MQL increases the intensity of normal stresses in the ploughing-dominant region making the tool more vulnerable to edge-chipping as compared to dry cutting under same parametric conditions. TiAlN coating initially protects the cutting edge from brittle fracture. After delamination, thick adhesion layer also protects the tool from fracture. As soon as adhered layer disappears partially or completely from the cutting edge, exposed substrate WC/6Co within the ploughing-dominant region experiences high normal stresses beyond its tolerable limit leading to chipping. Tools mostly experience first chipping by 80 – 120 mm length of cut.

Declaration of Competing Interest

The authors declare that they have no known competing financial interests or personal relationships that could have appeared to influence the work reported in this paper.

Acknowledgement

This research did not receive any specific grant from funding agencies in the public, commercial, or not-for-profit sectors.

References

[1] Tlusty J, Masood Z. Chipping and breakage of carbide tools. J. Eng. Ind. 1978;100: 403–12. https://doi.org/10.1115/1.3439454.

[2] Chen N, Li HN, Wu J, Li Z, Li L, Liu G, et al. Advances in micro milling: From tool fabrication to process outcomes. Int. J. Mach. Tools Manuf. 2021;160:103670. https://doi.org/10.1016/j.ijmachtools.2020.103670.

[3] Sun Y, Gong YD, Wen XL, Yin GQ, Meng FT. Micro milling characteristics of LS-WEDM fabricated helical and corrugated micro end mill. Int. J. Mech. Sci. 2020; 167:105277. https://doi.org/10.1016/j.ijmecsci.2019.105277.

[4] Singh KK, Kartik V, Singh R. Modeling dynamic stability in high-speed micromilling of Ti–6Al–4V via velocity and chip load dependent cutting coefficients. Int. J. Mach. Tools Manuf. 2015;96:56–66. https://doi.org/10.1016/j.ijmachtools.2015.06.002.

[5] Dib MHM, Duduch JG, Jasinevicius RG. Minimum chip thickness determination by means of cutting force signal in micro endmilling. Precis. Eng. 2018;51:244–62. https://doi.org/10.1016/j.precisioneng.2017.08.016.

[6] Aramcharoen A, Mativenga PT, Yang S, Cooke KE, Teer DG. Evaluation and selection of hard coatings for micro milling of hardened tool steel. Int. J. Mach. Tools Manuf. 2008;48:1578–84. https://doi.org/10.1016/j.ijmachtools.2008.05.011.

[7] Ucun İ, Aslantas K, Bedir F. An experimental investigation of the effect of coating material on tool wear in micro milling of Inconel 718 super alloy. Wear 2013;300: 8–19. https://doi.org/10.1016/j.wear.2013.01.103.

[8] Oliaei SN, Karpat Y. Influence of tool wear on machining forces and tool deflections during micro milling. Int. J. Adv. Manuf. Technol. 2015;84:1963–80. https://doi.org/10.1007/s00170-015-7744-4.

[9] Lu X, Jia Z, Wang H, Si L, Liu Y, Wu W. Tool wear appearance and failure mechanism of coated carbide tools in micro-milling of Inconel 718 super alloy. Ind. Lubr. Tribol. 2016;68:267–77. https://doi.org/10.1108/ILT-07-2015-0114.

[10] Lu X, Wang F, Jia Z, Si L, Zhang C, Liang SY. A modified analytical cutting force prediction model under the tool flank wear effect in micro-milling nickel-based superalloy. Int. J. Adv. Manuf. Technol. 2017;91:3709–16. https://doi.org/10.1007/s00170-017-0001-2.

[11] Miranda M, Serje D, Pacheco J, Bris J. Tool edge radius wear and material removal rate performance charts for titanium micro-milling. Int. J. Precis. Eng. Manuf. 2018;19:79–84. https://doi.org/10.1007/s12541-018-0009-z.

[12] Jahan MP, Ma J, Hanson C, Arbuckle GK. Tool wear and resulting surface finish during micro slot milling of polycarbonates using uncoated and coated carbide tools. Proc. Inst. Mech. Eng., Part B: J. Eng. Manuf. 2019;234:52–65. https://doi.org/10.1177/0954405419862479.

[13] Alhadeff LL, Marshall MB, Curtis DT, Slatter T. Protocol for tool wear measurement in micro-milling. Wear 2019;420-421:54–67. https://doi.org/10.1016/j.wear.2018.11.018.

[14] Dadgari A, Huo D, Swailes D. Investigation on tool wear and tool life prediction in micro-milling of Ti-6Al-4V. Nanotechnol. Precis. Eng. 2018;1:218–25. https://doi.org/10.1016/j.npe.2018.12.005.

[15] Vipindas K, Mathew J. Wear behavior of TiAlN coated WC tool during micro end milling of Ti-6Al-4V and analysis of surface roughness. Wear 2019;424-425: 165–82. https://doi.org/10.1016/j.wear.2019.02.018.

[16] Wang Y, Zou B, Wang J, Wu Y, Huang C. Effect of the progressive tool wear on surface topography and chip formation in micro-milling of Ti–6Al–4V using Ti(C7N3)-based cermet micro-mill. Tribol. Int. 2020;141:105900. https://doi.org/10.1016/j.triboint.2019.105900.

[17] Zhang X, Yu T, Zhao J. Surface generation modeling of micro milling process with stochastic tool wear. Precis. Eng. 2020;61:170–81. https://doi.org/10.1016/j.precisioneng.2019.10.015.

[18] Ziberov M, de Oliveira D, da Silva MB, Hung WNP. Wear of TiAlN and DLC coated microtools in micromilling of Ti-6Al-4V alloy. J. Manuf. Processes 2020;56: 337–49. https://doi.org/10.1016/j.jmapro.2020.04.082.

[19] Varghese A, Kulkarni V, Joshi SS. Tool life stage prediction in micro-milling from force signal analysis using machine learning methods. ASME J. Manuf. Sci. Eng. 2020;143. https://doi.org/10.1115/1.4048636.

[20] An Q, Cai C, Zou F, Liang X, Chen M. Tool wear and machined surface characteristics in side milling Ti6Al4V under dry and supercritical CO2 with MQL conditions. Tribol. Int. 2020;151:106511. https://doi.org/10.1016/j.triboint.2020.106511.

[21] Silva LC, da Silva MB. Investigation of burr formation and tool wear in micromilling operation of duplex stainless steel. Precis. Eng. 2019;60:178–88. https://doi.org/10.1016/j.precisioneng.2019.08.006.

[22] Khaliq W, Zhang C, Jamil M, Khan AM. Tool wear, surface quality, and residual stresses analysis of micro-machined additive manufactured Ti–6Al–4V under dry and MQL conditions. Tribol. Int. 2020;151:106408. https://doi.org/10.1016/j.triboint.2020.106408.

[23] Anand Krishnan N, Mathew J. Studies on wear behavior of AlTiN-coated WC tool and machined surface quality in micro endmilling of Inconel 718. Int. J. Adv. Manuf. Technol. 2020;110:291–307. https://doi.org/10.1007/s00170-020-05875-w. 291–307.

[24] Yang X, Cheng X, Li Y, Zheng G, Xu R. Machinability investigation and sustainability analysis of minimum quantity lubrication–assisted micro-milling process. Proc. Inst. Mech. Eng., Part B: J. Eng. Manuf. 2020;234:1388–401. https://doi.org/10.1177/0954405420921727.

[25] Wu X, Li L, He N, Zhao G, Jiang F, Shen J. Study on the tool wear and its effect of PCD tool in micro milling of tungsten carbide. Int. J. Refract. Met. Hard Mater 2018;77:61–7. https://doi.org/10.1016/j.ijrmhm.2018.07.010.

[26] Móricz L, Viharos ZJ, Németh A, Szépligeti A, Büki M. Off-line geometrical and microscopic & on-line vibration based cutting tool wear analysis for micro-milling of ceramics. Measurement 2020;163:108025. https://doi.org/10.1016/j.measurement.2020.108025.

[27] Manso CS, Thom S, Uhlmann E, de Assis CL, del Conte EG. Tool wear modelling using micro tool diameter reduction for micro-end-milling of tool steel H13. Int. J. Adv. Manuf. Technol. 2019;105:2531–42. https://doi.org/10.1007/s00170-019-04575-4.

[28] Wang Y, Zou B, Huang C, Liu Z, Yao P. The micro-cutting performance OF Cermet and coated WC Micro-mills in machining OF TC4 Alloy micro-grooves. Int. J. Adv. Manuf. Technol. 2018;96:1403–14. https://doi.org/10.1007/s00170-018-1638-1.

[29] Hajiahmadi S. Burr size investigation in micro milling of stainless steel 316L. Int. J. Lightweight Mater. Manuf. 2019;2:296–304. https://doi.org/10.1016/j.ijlmm.2019.07.004.

[30] Liang X, Liu Z. Experimental investigations on effects of tool flank wear on surface integrity during orthogonal dry cutting of Ti-6Al-4V. Int. J. Adv. Manuf. Technol. 2017;93:1617–26. https://doi.org/10.1007/s00170-017-0654-x.

[31] Sorgato M, Bertolini R, Bruschi S. On the correlation between surface quality and tool wear in micro–milling of pure copper. J. Manuf. Processes 2020;50:547–60. https://doi.org/10.1016/j.jmapro.2020.01.015.

[32] Arefin S, Zhang XQ, Neo DW, Kumar AS. Effects of cutting edge radius in vibration assisted micro machining. Int. J. Mech. Sci. 2021;208:106673. https://doi.org/10.1016/j.ijmecsci.2021.106673.

[33] Rahul Y, Vipindas K, Mathew J. Methodology for prediction of sub-surface residual stress in micro end milling of ti-6al-4v alloy. J. Manuf. Processes 2021;62:600–12. https://doi.org/10.1016/j.jmapro.2020.12.031.

[34] Zhang X, Yu T, Dai Y, Qu S, Zhao J. Energy consumption considering tool wear and optimization of cutting parameters in micro milling process. Int. J. Mech. Sci. 2020;178:105628. https://doi.org/10.1016/j.ijmecsci.2020.105628.

[35] Zhang X, Yu T, Xu P, Zhao J. An intelligent sustainability evaluation system of micro milling. Rob. Comput. Integr. Manuf. 2022;73:102239. https://doi.org/10.1016/j.rcim.2021.102239.

[36] dos Santos AG, da Silva MB, Jackson MJ. Tungsten carbide micro-tool wear when micro milling UNS S32205 duplex stainless steel. Wear 2018;414-415:109–17. https://doi.org/10.1016/j.wear.2018.08.007.
[37] Usui E, Shirakashi T, Kitagawa T. Analytical prediction of cutting tool wear. Wear 1984;100:129–51. https://doi.org/10.1016/0043-1648(84)90010-3.
[38] Mittal R, Maheshwari C, Kulkarni SS, Singh R. Effect of progressive tool wear on the evolution of the dynamic stability limits in high-speed micromilling of Ti-6Al-4V. ASME J. Manuf. Sci. Eng. 2019;141. https://doi.org/10.1115/1.4044713.
[39] Vazquez E, Gomar J, Ciurana J, Rodríguez CA. Analyzing effects of cooling and lubrication conditions in micromilling of Ti6Al4V. J. Cleaner Prod. 2015;87:906–13. https://doi.org/10.1016/j.jclepro.2014.10.016.
[40] Wang Y, Zou B, Huang C. Tool wear mechanisms and micro-channels quality in micro-machining of Ti-6Al-4V alloy using the Ti(C7N3)-based cermet micro-mills. Tribol. Int. 2019;134:60–76. https://doi.org/10.1016/j.triboint.2019.01.030.
[41] Toropov A, Ko S-L. Prediction of tool-chip contact length using a new slip-line solution for orthogonal cutting. Int. J. Mach. Tools Manuf. 2003;43:1209–15. https://doi.org/10.1016/S0890-6955(03)00155-X.
[42] Hu C, Zhang W, Zhuang K, Zhou J, Ding H. On the steady-state workpiece flow mechanism and force prediction considering piled-up effect and dead metal zone formation. ASME J. Manuf. Sci. Eng. 2020;143. https://doi.org/10.1115/1.4048952.
[43] Son SM, Lim HS, Ahn JH. Effects of the friction coefficient on the minimum cutting thickness in micro cutting. Int. J. Mach. Tools Manuf. 2005;45:529–35. https://doi.org/10.1016/j.ijmachtools.2004.09.001.
[44] Rezaei H, Sadeghi MH, Budak E. Determination of minimum uncut chip thickness under various machining conditions during micro-milling of ti-6al-4v. Int. J. Adv. Manuf. Technol. 2017;95:1617–34. https://doi.org/10.1007/s00170-017-1329-3.
[45] Malekian M, Mostofa MG, Park SS, Jun MBG. Modeling of minimum uncut chip thickness in micro machining of aluminum. J. Mater. Process. Technol. 2012;212:553–9. https://doi.org/10.1016/j.jmatprotec.2011.05.022.
[46] Merchant ME. Mechanics of the metal cutting process. I. Orthogonal cutting and a type 2 chip. J. Appl. Phys. 1945;16:267–75. https://doi.org/10.1063/1.1707586.
[47] Wu Y, Chen N, Bian R, He N, Li Z, Li L. Investigations on burr formation mechanisms in micro milling of high-aspect-ratio titanium alloy Ti-6Al-4V structures. Int. J. Mech. Sci. 2020;185:105884. https://doi.org/10.1016/j.ijmecsci.2020.105884.
[48] Liao Z, Axinte DA. On chip formation mechanism in orthogonal cutting of bone. Int. J. Mach. Tools Manuf. 2016;102:41–55. https://doi.org/10.1016/j.ijmachtools.2015.12.004.
[49] Wang Y, Zou B, Huang C, Qi H, Song J. Feasibility study of THE Ti(C7N3)-based cermet Micro-mill based on dynamic fatigue behavior and modeling of the contact stress distribution on the round cutting edge. Int. J. Mech. Sci. 2019;155:143–58. https://doi.org/10.1016/j.ijmecsci.2019.02.038.
[50] Kita Y, Ido M, Kawasaki N. A study of metal flow ahead of tool face with large negative rake angle. J. Eng. Ind. 1982;104:319–25. https://doi.org/10.1115/1.3185836.
[51] Usui E, Takeyama H. A Photoelastic analysis of Machining stresses. ASME J. Eng. Ind. 1960;82:303–7. https://doi.org/10.1115/1.3664233.
[52] Mesquita RMD, Barata Marques MJM. Experimental determination of the dynamic shear stress in metal cutting. J. Mater. Process. Technol. 1992;33:229–46. https://doi.org/10.1016/0924-0136(92)90210-J.
[53] Rahman MA, Rahman M, Mia M, Gupta MK, Sen B. Ahmed A. Investigation of the specific cutting energy and its effect in shearing dominant precision micro cutting. J. Mater. Process. Technol. 2020;283:116688. https://doi.org/10.1016/j.jmatprotec.2020.116688.
[54] Zhao Z, To S, Zhu Z, Yin T. A theoretical and experimental investigation of cutting forces and spring back behaviour of Ti6Al4V alloy in ultraprecision machining of microgrooves. Int. J. Mech. Sci. 2020;169:105315. https://doi.org/10.1016/j.ijmecsci.2019.105315.
[55] Maity KP, Das NS. A class of slipline field solutions for metal machining with sticking–slipping zone including elastic contact. Mater. Des. 2007;28:2310–7. https://doi.org/10.1016/j.matdes.2006.07.014.
[56] Saha S, Deb S, Bandyopadhyay PP. An analytical approach to assess the variation of lubricant supply to the cutting tool during MQL assisted high speed micromilling. J. Mater. Process. Technol. 2020;285:116783. https://doi.org/10.1016/j.jmatprotec.2020.116783.
[57] Mark Benjamin D, Sabarish VN, Hariharan MV, Samuel Raj D. On the benefits of sub-zero air supplemented minimum quantity lubrication systems: An experimental and mechanistic investigation on end milling of Ti-6Al-4V alloy. Tribol. Int. 2018;119:464–73. https://doi.org/10.1016/j.triboint.2017.11.021. 473.
[58] Wojciechowski S, Matuszak M, Powałka B, Madajewski M, Maruda RW, Królczyk GM. Prediction of cutting forces during micro end milling considering chip thickness accumulation. Int. J. Mach. Tools Manuf. 2019;147:103466. https://doi.org/10.1016/j.ijmachtools.2019.103466.
[59] Rahman MA, Rahman M, Woon KS, Mia M. Episodes of chip formation in micro-to-nanoscale cutting of Inconel 625. Int. J. Mech. Sci. 2021;199:106407. https://doi.org/10.1016/j.ijmecsci.2021.106407.
[60] Sun Z, Zhang T, Li P, Wang S, To S, Wang H. Analytical modelling of the trans-scale cutting forces in diamond cutting of polycrystalline metals considering material microstructure and size effect. Int. J. Mech. Sci. 2021;204:106575. https://doi.org/10.1016/j.ijmecsci.2021.106575.
[61] Kieren-Ehses S, Böhme L, Morales-Rivas L, Lösch J, Kirsch B, Kerscher E, et al. The influence of the crystallographic orientation when micro machining commercially pure titanium: A size effect. Precis. Eng. 2021;72:158–71. https://doi.org/10.1016/j.precisioneng.2021.04.007.
[62] Melkote SN, Thangaraj AR. An enhanced end milling surface texture model including the effects of radial rake and primary relief Angles. ASME J. Eng. Ind. 1994;116:166–74. https://doi.org/10.1115/1.2901927.
[63] Ryu SH, Choi DK, Chu CN. Roughness and texture generation on end milled surfaces. Int. J. Mach. Tools Manuf. 2006;46:404–12. https://doi.org/10.1016/j.ijmachtools.2005.05.010.
[64] Muñoz-Escalona P, Maropoulos PG. A geometrical model for surface roughness prediction when face milling Al 7075-T7351 with square insert tools. J. Manuf. Syst. 2015;36:216–23. https://doi.org/10.1016/j.jmsy.2014.06.011.
[65] Klocke F, Lortz W, Trauth D. Analysis of the dynamic chip formation process in turning. Int. J. Mech. Sci. 2018;135:313–24. https://doi.org/10.1016/j.ijmecsci.2017.11.035.
[66] Liang X, Liu Z, Wang B. Physic-chemical analysis for high-temperature tribology of WC-6Co against Ti–6Al–4V by pin-on-disc method. Tribol. Int. 2020;146:106242. https://doi.org/10.1016/j.triboint.2020.106242.
[67] Miguélez MH, Soldani X, Molinari A. Analysis of adiabatic shear banding in orthogonal cutting of Ti alloy. Int. J. Mech. Sci. 2013;75:212–22. https://doi.org/10.1016/j.ijmecsci.2013.06.011.
[68] Ghosh G, Sidpara A, Bandyopadhyay PP. Fabrication of mechanically durable slippery surface on HVOF sprayed WC-Co coating. Surf. Coat. Technol. 2020;394:125886. https://doi.org/10.1016/j.surfcoat.2020.125886.
[69] Bartosik M, Rumeau C, Hahn R, Zhang ZL, Mayrhofer PH. Fracture toughness and structural evolution in the TiAlN system upon annealing. Sci. Rep. 2017;7. https://doi.org/10.1038/s41598-017-16751-1.
[70] Broitman E. Indentation hardness measurements at Macro-, Micro-, and Nanoscale: A critical overview. Tribol. Lett. 2016;65. https://doi.org/10.1007/s11249-016-0805-5.
[71] Wang Z, Yu B, Liu K, Yin Z, Yuan J, Zhu Y. Performance and wear mechanism of spark plasma sintered WC-based ultrafine cemented carbides tools in dry turning of Ti–6Al–4V. Ceram. Int. 2020;46:20207–14. https://doi.org/10.1016/j.ceramint.2020.05.101.